The Meteoritical Society

Meteoritics & Planetary Science 49, Nr 4, 503–525 (2014)
doi: 10.1111/maps.12282

Elemental, isotopic, and structural changes in Tagish Lake insoluble organic matter produced by parent body processes

C. M. O'D. ALEXANDER[1*], G. D. CODY[2], Y. KEBUKAWA[2], R. BOWDEN[2], M. L. FOGEL[2,5], A. L. D. KILCOYNE[3], L. R. NITTLER[1], and C. D. K. HERD[4]

[1]Department of Terrestrial Magnetism, Carnegie Institution of Washington, 5241 Broad Branch Road, Washington, District of Columbia 20015, USA
[2]Geophysical Laboratory, Carnegie Institution of Washington, 5251 Broad Branch Road, Washington, District of Columbia 20015, USA
[3]Advanced Light Source, Lawrence Berkeley National Laboratory, Berkeley, California 94720, USA
[4]Department of Earth and Atmospheric Sciences, University of Alberta, Edmonton, AB, T6G 2E3, Canada
[5]Present Address: School of Natural Sciences, University of California at Merced, Merced, California 95343, USA
[*]Corresponding author. E-mail: alexande@dtm.ciw.edu

(Received 29 April 2013; revision accepted 06 February 2014)

Abstract–Here, we present the results of a multitechnique study of the bulk properties of insoluble organic material (IOM) from the Tagish Lake meteorite, including four lithologies that have undergone different degrees of aqueous alteration. The IOM C contents of all four lithologies are very uniform and comprise about half the bulk C and N contents of the lithologies. However, the bulk IOM elemental and isotopic compositions vary significantly. In particular, there is a correlated decrease in bulk IOM H/C ratios and δD values with increasing degree of alteration—the IOM in the least altered lithology is intermediate between CM and CR IOM, while that in the more altered lithologies resembles the very aromatic IOM in mildly metamorphosed CV and CO chondrites, and heated CMs. Nuclear magnetic resonance (NMR) spectroscopy, C X-ray absorption near-edge (XANES), and Fourier transform infrared (FTIR) spectroscopy confirm and quantitate this transformation from CR-like, relatively aliphatic IOM functional group chemistry to a highly aromatic one. The transformation is almost certainly thermally driven, and probably occurred under hydrothermal conditions. The lack of a paramagnetic shift in ^{13}C NMR spectra and 1s-σ* exciton in the C-XANES spectra, both typically seen in metamorphosed chondrites, shows that the temperatures were lower and/or the timescales were shorter than experienced by even the least metamorphosed type 3 chondrites. Two endmember models were considered to quantitatively account for the changes in IOM functional group chemistry, but the one in which the transformations involved quantitative conversion of aliphatic material to aromatic material was the more successful. It seems likely that similar processes were involved in producing the diversity of IOM compositions and functional group chemistries among CR, CM, and CI chondrites. If correct, CRs experienced the lowest temperatures, while CM and CI chondrites experienced similar more elevated temperatures. This ordering is inconsistent with alteration temperatures based on mineralogy and O isotopes.

INTRODUCTION

The dominant organic component in chondritic meteorites is a macromolecular insoluble organic material (IOM) whose origin is still uncertain. Large D and ^{15}N enrichments in the IOM have traditionally been interpreted as indicating that at least a significant component of the IOM formed in the interstellar medium (ISM) (Robert and Epstein 1982; Kerridge 1983; Yang and Epstein 1983, 1984) or formed from ISM material (Cody et al. 2011). However, an interstellar heritage for the IOM has been questioned

(Remusat et al. 2006; Gourier et al. 2008; Nuth et al. 2008) because the conditions in some regions of the solar nebula may have been quite similar to those in the ISM. Hence, it may be necessary to find indirect criteria for determining where the IOM formed.

If the IOM was largely or wholly inherited from the protosolar molecular cloud, one might expect that (1) IOM-like material would have been distributed throughout the cooler parts of the early solar nebula; (2) it would have been accreted by all primitive solar system bodies; (3) its abundance relative to presolar grains would be constant in all primitive materials; and (4) all IOM in chondrites would have features that can be traced back to a common, primordial material. Criteria 1–3 are only briefly discussed here as it is with criterion 4 that this article is primarily concerned.

Alexander (2005) concluded that the relative abundances of IOM and presolar (Xe-HL carrying) nanodiamonds are fairly constant in the least metamorphosed chondrites. IOM abundances relative to other presolar grains are much less certain (e.g., Huss et al. 2003; Davidson et al. 2009). There is some evidence that IOM-like material was widespread in the early solar nebula. In terms of its isotopic composition, functional group chemistry, morphology, and Raman spectral features, the organic matter in interplanetary dust particles (IDPs), which may come from comets, closely resembles that of IOM in the most primitive chondrites (Messenger 2000; Flynn et al. 2003; Keller et al. 2004; Busemann et al. 2006; Matrajt et al. 2012). Some comet Wild 2 organic particles also resemble meteoritic IOM (Sandford et al. 2006; Cody et al. 2008a, 2011; Matrajt et al. 2008; De Gregorio et al. 2010, 2011). Finally, the average elemental composition of comet Halley CHON particles (Kissel and Krueger 1987) resembles the compositions of IOM in the most primitive chondrites (Alexander et al. 2007).

The principal objection to a common origin for all IOM is the tremendous diversity of IOM elemental and isotopic compositions found in chondrites (Robert and Epstein 1982; Kerridge 1983; Yang and Epstein 1983, 1984; Alexander et al. 1998, 2007, 2010; Oba and Naraoka 2009). The unresolved question is whether nebula (heating and irradiation) and/or parent body (thermal metamorphism, shock heating, and hydrothermal alteration) processes can account for these variations.

With increasing thermal metamorphism in CV, CO, and ordinary (OC) chondrites, there are similar changes in IOM Raman spectra (Quirico et al. 2003, 2009; Bonal et al. 2006, 2007; Busemann et al. 2007), nanostructure as determined by transmission electron microscopy (Le Guillou et al. 2012), elemental compositions (Alexander et al. 1998, 2007, 2010), and molecular structure determined via C X-ray absorption near-edge spectroscopy (C-XANES) (Cody et al. 2008b). This is at least consistent with all three groups having accreted similar primordial IOM material. Furthermore, it has been shown experimentally that purely thermal metamorphism will convert the molecular structure of primitive IOM (e.g., that of the CM2 Murchison), into a structure that is nearly identical to that of metamorphosed IOM (e.g., that of the CV3 Vigarano) (Cody et al. 2008b). The severely heated carbonaceous material in enstatite (EC) chondrites also appears consistent with the CV-CO-OC trends, suggesting that they too accreted an IOM-like material (Alexander et al. 1998; Le Guillou et al. 2012; Piani et al. 2012). However, differences in the variations in the isotopic compositions of the IOM, particularly for H, among the CVs, COs, and OCs mean that there must have been significant differences in conditions during metamorphism if they had a common parental IOM (Alexander et al. 2007, 2010). These chondrite groups have no unmetamorphosed members and at present, it is not possible to extrapolate backwards to infer their initial IOM compositions. Thus, while a strong case can be made that the primordial IOM accreted by the CVs, COs, and OCs did resemble the IOM in the unmetamorphosed type 1 and 2 chondrites, it still remains unclear just how chemically and isotopically similar they were.

It is not, perhaps, surprising that thermal metamorphism under varying conditions will have modified the IOM in somewhat different ways. Indeed, recent work by Kebukawa et al. (2011) reported molecular diversity that is most readily explained by different conditions during metamorphism. On the other hand, the extent to which IOM was modified by the aqueous alteration experienced by type 1 and 2 chondrites is more controversial. For instance, based on infrared (IR) spectroscopy of CI, CM, and CR IOM, Orthous-Daunay et al. (2013) argue that the structural variations in IOM between these chondrite groups cannot be accounted for by aqueous alteration, but must reflect modest variations in the nature of the IOM that they accreted. There are significant differences in IOM composition between CI, CM, and CR chondrites, but less variation within the groups.

The IOM in CRs is generally the most isotopically anomalous (Robert and Epstein 1982; Yang and Epstein 1983; Alexander et al. 1998, 2007) and aliphatic (Cody and Alexander 2005) of the CI-CM-CRs. The IOM in CRs is quite uniform in composition, except for some variation in H and N isotopic compositions. These isotopic variations do not seem to be a function of petrologic type. IOM in the CMs is slightly more aromatic and less isotopically anomalous than the CRs.

However, like the CRs, there is generally little variation in elemental composition among the CMs, although modest differences in H and N isotopes do seem to be a function of alteration conditions (Alexander et al. 2007, 2013b). The one exception is Bells that has among the most D- and ^{15}N-rich IOM compositions of any type 1 or 2 chondrite, but otherwise, its IOM resembles a typical CM (Alexander et al. 2007; Cody et al. 2008c). Bells appears to be an anomalous CM (Mittlefehldt 2002) that has experienced an atypical style of alteration (Brearley 1995). The IOM in CI chondrites is intermediate between typical CM and CR chondrites in terms of aromaticity (Cody and Alexander 2005), and elemental and isotopic composition (Alexander et al. 2007).

The best estimates for the alteration conditions in CMs, CIs, and CRs are that they were quite mild, 0–150 °C (Zolensky et al. 1989; Brearley 2006; Guo and Eiler 2007; Guo 2009), and it has often been implicitly assumed that little modification in IOM could have taken place under these conditions. However, if these meteorite groups all accreted a common primordial IOM, the variations in their current IOM compositions and functional group chemistries require extensive molecular structural modification (Cody and Alexander 2005).

Hydrothermal experiments conducted at approximately 300 °C have shown that there can be rapid and extensive modification in IOM molecular structure, H/C ratio, and H isotopic compositions (Yabuta et al. 2007; Oba and Naraoka 2009). The change in H isotopic composition is either through isotopic exchange and/or elimination of D-rich functional groups. The rates of change in H isotopic composition in these IOM hydrothermal experiments are roughly consistent with H isotope exchange between water and simple PAHs at similar temperatures and under nonneutral PH conditions (with or without the presence of clay catalysts) (Alexander et al. 1982; Oba and Naraoka 2003). Extrapolation of the PAH exchange rate data to low temperatures suggests that water-IOM H isotope exchange could occur on geologically short timescales above approximately 25–50 °C (Alexander et al. 2010). Thus, it is at least plausible that some or all of the differences in H isotopic compositions within and between the CM, CI, and CR chondrites are the result of isotopic exchange between IOM and water. Whether it is possible to achieve the variations in IOM aromaticity and elemental compositions that are seen among these chondrite groups at such low temperatures still remains unclear.

Of all the known C1–2s, the ungrouped C2 Tagish Lake has the most unusual IOM. Tagish Lake has a mineralogy, bulk O isotope, and bulk chemical composition that is intermediate between CI and CM chondrites (Brown et al. 2000). The two major lithologies of Tagish Lake experienced extensive hydrothermal alteration under relatively oxidizing conditions—magnetite, and Fe-rich phyllosilicates and carbonates are abundant (Zolensky et al. 2002; Greshake et al. 2005). The IOM in previous studies of Tagish Lake has the highest aromaticity (Pizzarello et al. 2001; Cody and Alexander 2005), and the lowest bulk H/C ratio and δD value (Alexander et al. 2007) of any C1–2. The hydrothermal experiments of Yabuta et al. (2007) converted the molecular structure of Murray (CM2) IOM into something that closely resembled the molecular structure of Tagish Lake IOM. However, these were relatively high temperature experiments, the spectral resemblance is not exact, and the fact that there is some resemblance does not necessarily mean that the Tagish Lake IOM must have formed by hydrothermal alteration of a more primitive IOM material.

A more convincing case has been made by Herd et al. (2011) in their study of the soluble organic material and IOM from four distinct Tagish Lake lithologies. These lithologies experienced different degrees of parent body aqueous alteration (increasing in the order, by specimen name: 5b, 11h, 11i, 11v) (Blinova et al. 2014b). Nevertheless, all the lithologies have the same Δ^{17}O values as the original Tagish Lake samples (Herd et al. 2012), and exhibit many mineralogical, petrological, and bulk compositional similarities (Blinova et al. 2014a, 2014b). Hence, it is clear that all lithologies are from the Tagish Lake parent body and none are xenolithic clasts. The advantage of having samples from the same meteorite and the same parent body is that any variations in IOM composition that are found must be due to parent body processes. The IOM in these lithologies exhibited correlated decreases in δD and H/C, and increases in aromatic C fraction with increasing degree of aqueous alteration from 5b to 11v.

Here, we use new IOM results and a detailed analysis of the IOM data briefly described by Herd et al. (2011) in their supporting online material to conclude that indeed hydrothermal alteration in the Tagish Lake parent body did transform a CR-like IOM into the very aromatic IOM previously found in the dominant Tagish Lake lithologies (Pizzarello et al. 2001; Cody and Alexander 2005).

METHODS

IOM Isolation

This study involves specimens 5b, 11h, 11i, and 11v (the latter collected as disaggregated material) that were

part of the pristine suite of Tagish Lake material described by Herd et al. (2011). The Tagish Lake meteorite specimens were transferred from storage in a −28 °C research grade freezer to a −18 °C walk-in freezer for subsampling for both soluble organic analysis (Glavin et al. 2012; Hilts et al. 2014) and insoluble organic matter studies (Herd et al. 2011; this study). Subsampling of interior material was carried out using sterile scalpels that had been rinsed in ultrapure water. Most samples (with the exception of 11v) used in IOM isolation were residues after extraction of amino acids (water reflux at 100 °C for 6 h; Hilts et al. 2014). An earlier unpublished experiment with two CR chondrites suggests that the amino acid extraction does not significantly modify the elemental or isotopic compositions of IOM.

The IOM residues were prepared and analyzed using the same methods as described in Alexander et al. (2007, 2010). Briefly, the CsF-HF technique was used in which the powdered samples are first leached with 2N HCl, followed by rinsing with milliQ water and dioxane, and then shaken in the presence of two immiscible liquids, a CsF-HF solution (1.6–17 g mL^{-1}) and dioxane. When liberated from its mineral matrix, the IOM collects at the interface of the CsF-HF solution and the dioxane, while the denser minerals sink to the bottom. After centrifugation, the IOM is pipetted off and rinsed with 2N HCl, milliQ water and then dioxane, before being dried down at <30–50 °C. The previous reflux treatment and the repeated washing with aqueous solutions and dioxane during IOM isolation should have effectively removed most soluble organic compounds known to be present in chondrites.

Elemental and Isotopic Analysis

In addition to the IOM samples, aliquots of powders from the four bulk lithologies were analyzed for their bulk H, C, and N abundances and isotopic compositions. All samples were stored in a desiccator for at least several days prior to analysis.

Elemental and isotopic analyses for H were made with a Thermo Finnigan Delta^{plus}XL mass spectrometer; for C and N, we used a Thermo Delta V Plus isotope ratio mass spectrometer. Sample gases were introduced into the mass spectrometer via a Conflo III interface connected to either: a CE Instruments NA 2500 series elemental analyzer (EA) for C and N analyses, or a Thermo Finnigan thermal conversion elemental analyzer (TC/EA) for H analyses. For all analyses, internal working gas standards were analyzed with every sample, and external standards were analyzed at regular intervals to monitor the accuracy of the measured isotopic ratios and elemental compositions. A correction for H_3^+ was applied to the H measurements; its magnitude was determined at the beginning of the day. For the H analyses, a He-flushed zero-blank autosampler was used to reduce the amount of water adsorbed from the atmosphere. Typical sample sizes were 0.2–0.4 mg.

The measurement precision for elemental abundances is typically of the order 1–3% of the reported values. Because C and N are measured in the same samples, the precision of measured N/C ratios is typically about 1% of the reported values. The precision of C and N isotope measurements is generally 0.1–0.3‰. The accuracy of the H isotope measurements is more difficult to assess because it decreases with increasing D enrichment, and because there is a small memory effect associated with the measurements. Sample heterogeneity is also a potential source of uncertainty in all the measurements.

^{13}C and ^{1}H NMR Spectroscopy

Solid-state nuclear magnetic resonance (NMR) provides a powerful means of revealing, quantitatively, the organic functional group distribution in complex organic solids, particularly if direct polarization methods are employed. In the present case, there was insufficient IOM available to achieve acceptable signal to noise (S/N) spectra using direct polarization (DP). In many cases, cross polarization methods (^{1}H to ^{13}C) greatly enhance S/N; thus, variable amplitude cross polarization (VACP) magic angle spinning (MAS) ^{13}C NMR was employed. It has been previously shown that when applied to IOM, VACP with a 4.5 ms contact time yields nearly identical functional group distributions as is determined via DP NMR, albeit with a slight enhancement of aliphatic C intensity over aromatic C intensity (Cody et al. 2002; Cody and Alexander 2005).

All NMR analyses were performed with a Varian Chemagnetics Infinity NMR operating at a static magnetic field strength of 7.05 T where the resonant frequencies of ^{1}H and ^{13}C are 300.2 MHz and 75.5 MHz, respectively. All ^{13}C solid-state NMR experiments were performed with a 5 mm Chemagnetics double resonance probe. Owing to the relatively small quantities of sample available for analysis, variable amplitude ^{1}H-^{13}C cross polarization employing a 4 μs 90° pulse on ^{1}H was followed by a 4.5 ms contact pulse on ^{1}H and ^{13}C. High power ^{1}H decoupling ($\omega_1/2\pi$ = 62.5 KHz) was applied during signal acquisition. These parameters have been shown to be optimum for maximum signal intensity and minimal distortion due to functional group variations in T_{CH} and $T_{1\rho}$ (Cody and Alexander 2005). Magic Angle Sample spinning (MAS)

was performed at a frequency ($\omega_r/2\pi$) of 11.5 KHz. In each case, 10^5 acquisitions with a recycle delay of 1 s were employed. The ^{13}C spectral frequencies are referenced to the methyl frequency for tetramethylsilane being defined as 0 ppm.

The ^1H NMR analyses were performed with a 2.5 mm Chemagnetics double resonance probe. To suppress background ^1H signal from various probe components, all analyses employed the DEPTH sequence, wherein any ^1H experiencing a pulse width of 45 °C or less is averaged to zero. The experimental parameters include a 3 μs 90° ^1H pulse, a 200 KHz spectral width, relatively fast MAS ($\omega_r/2\pi$ = 22 KHz), and a recycle delay of 1 s. The number of acquisitions was 6400 and the proton frequency was referenced to methyl H frequency for tetramethylsilane being defined at 0 ppm.

Fourier Transform Infrared Micro-Spectroscopy

Small amounts of IOM from each lithology were mixed with high-purity S powder and placed on a hot plate, so that the S melted. The molten S droplets were subsequently cooled and attached to epoxy stubs using a dab of cyanoacrylate cement. Sections of 1.5–2 μm thickness were prepared with a LEICA microtome equipped with a glass knife. The sections were deposited onto BaF_2 disks (13 × 1 mm) with a small amount of pure water, and the S was subsequently sublimed away with mild heating (<100 °C, <1 h).

IR absorption spectra were collected with a Fourier transform IR microspectrometer (Micro FTIR; Jasco FT/IR-6300 + IMV4000) with a ceramic IR light source, a Ge-coated KBr beam splitter, a mercury-cadmium-telluride (MCT) detector, and ×10 or ×16 Cassegrainian mirrors. During analysis, the microscope and the Fourier transform infrared (FTIR) were continuously purged with dry N_2. From 512 to 2048 scans of IR transmission spectra were accumulated with a wave number resolution of 4 cm^{-1}, in the wave number range of 4000–700 cm^{-1}, using 20 × 20 to 100 × 100 μm^2 apertures depending on the sample size. Background spectra were acquired through the BaF_2 plate adjacent to the samples with the same aperture dimensions. Several different areas were analyzed for each sample, and all spectra were averaged for each sample to obtain the reported intensity ratios.

The C=O/C=C peak intensity ratios were determined from the peak areas of the bands between 1650 and 1800 cm^{-1} (C=O), and 1500 and 1650 cm^{-1} (C=C), relative to a linear baseline determined between 1500 and 1800 cm^{-1}. The aliphatic asymmetric CH_2 and CH_3 peak intensities were determined from the peak areas at 2880–2940 cm^{-1} and 2940–3000 cm^{-1}, respectively, and aromatic CH (aro-CH) stretch intensity was determined from the peak areas at 3020–3080 cm^{-1}. Both the aromatic and aliphatic C–H intensities used a polynomial baseline between 2700 and 3200 cm^{-1}. The quoted errors are the standard deviations of the FTIR analyses for each sample. The peak areas were determined by Gaussian fits using a similar approach to previous studies (e.g., Dartois et al. 2007; Orthous-Daunay et al. 2013). The functional group molecular ratio of CH_2/CH_3 (N_{CH_2}/N_{CH_3}) was calculated from the absorption intensity ratios using the equation

$$N_{CH_2}/N_{CH_3} = C \times (Abs_{CH_2})/(Abs_{CH_3}),$$

where Abs_{CH_2} and Abs_{CH_3} are the areas under the CH_2 and CH_3 absorption peaks. Estimates of the values of the constant C vary from 1.19 to 1.62 (Nakanishi and Solomon 1977; Ristein et al. 1998; Dartois et al. 2007; Orthous-Daunay et al. 2013). Hence, here we have used a value of 1.4 for C, recognizing that there may be at least an approximately 20% systematic error in the absolute ratios, but much less uncertainty in any relative changes in the ratios.

Carbon X-Ray Absorption Near-Edge Spectroscopy

Ultra-thin IOM sections, 100–150 nm thick were prepared from the same S-embedded samples described above using a diamond knife and a Leica Ultracut ultramicrotome. These sections were then transferred to SiO-coated TEM grids and gently heated (approximately 60 °C) until the S had sublimed off the grid.

All X-ray absorption near-edge spectroscopy (XANES) analyses were performed with the scanning transmission X-ray microscope at beam line 5.3.2.2 at the Advanced Light Source, Lawrence Berkeley Laboratory (Kilcoyne et al. 2003). BL5.3.2.2 employs a bending magnet providing a useful photon range spanning approximately 250–700 eV, with a maximum photon flux of 10^7 photons s^{-1}. Energy selection on BL5.3.2.2 is performed with a low dispersion spherical grating monochromator affording an energy resolution of 5000. Beam focusing utilizes Fresnel zone plate optics providing a theoretical spot size down to 25 nm; in optimum cases, smaller structures (approximately 15 nm) can be resolved. Maximum scanning rates for BL5.3.2.2 is 12 Hz, with a scanning range of 4000 × 2000 pixels covering a region up to 20 × 4 mm, with a minimum step size 2.5 nm. Sample position precision during spectra acquisition is better than 50 nm (Kilcoyne et al. 2003).

The C-XANES spectra were acquired via a multispectral or "Stacks" imaging method (Jacobsen et al. 2000). The "Stacks" method relies on the

Table 1. The results of elemental and isotopic analyses of IOM separated from the four Tagish Lake lithologies. The atomic ratios have all been multiplied by 100.

	C Yield[b] (wt%)	C[c] (wt%)	H/C (atom)	N/C (atom)	O/C (atom)	δD (‰)	$\delta^{13}C$ (‰)	$\delta^{15}N$ (‰)	$\delta^{18}O$ (‰)
Original[a]		67.5	33.7	4.28 ± 0.002	17 ± 1	596 ± 4	−14.2 ± 0.1	73 ± 2	12.5 ± 0.5
11v	1.67	66.2	45.6	4.20	13	789	−13.3	60	7.4
11v(2)	1.87	70.6	42.7	3.97		840	−13.3	56	
Mean	**1.77 ± 0.14**		**44.1 ± 2.1**	**4.1 ± 0.2**		**815 ± 36**	**−13.3 ± 0.0**	**58 ± 3**	
11i	1.86	70.0	52.7	4.45	26	1007	−13.1	56	12.6
11i(2)	1.79	71.7	49.2	4.04		977	−13.4	50	
Mean	**1.82 ± 0.05**		**50.9 ± 2.5**	**4.2 ± 0.3**		**992 ± 21**	**−13.3 ± 0.2**	**53 ± 4**	
11h	**1.86**	**66.0**	**59.4**	**4.2**		**1470**	**−14.3**	**57**	
5b	1.86	63.8	76.6	4.42	19	1834	−14.5	61	11.0
5b(2)	1.31	67.1	67.8	4.04		1854	−14.9	54	
Mean	**1.58 ± 0.39**		**72.2 ± 6.3**	**4.2 ± 0.3**		**1844 ± 14**	**−14.7 ± 0.3**	**57 ± 5**	

[a]Data for Tagish Lake from Alexander et al. (2007).
[b]The yield of IOM C in the bulk samples.
[c]The C contents of the residues.
Bold type differentiates the averages from the individual measurements.

acquisition of a series of pixelated X-ray absorption images over a range of energies that span a given XANES region. This generates an aligned hyperspectral data cube where every pixel contains a complete XANES spectrum. In the fine structure portions of the near-edge region (283–296 eV), the energy step size (ΔE) employed here was 0.1 eV; in the less featured pre-edge (278–283 eV) and postedge (296–301 eV) regions, energy steps of 0.5 eV provided sufficient spectral resolution. The final span of extended X-ray absorption structure (EXAFS) oscillations decaying down to the slope of the atomic C absorption (301–340 eV) is adequately covered with energy steps of 2 eV. In all cases, the acquisition time per energy step was 1.5 ms.

The C-XANES spectra presented here are averages over a large number of pixels. In this study, 50 × 50 pixel regions with step sizes of 200 nm (corresponding to an area of 10 × 10 μm) were hyperspectrally imaged. Typically, roughly one third of the pixels correspond to open areas (enabling acquisition of the normalization or I_0 spectrum). Consequently, the C-XANES spectra are the averages of approximately 1700 individual pixels normalized to the average of approximately 800 I_0 pixels, i.e., as $-\log[(\Sigma(I)/n)/(\Sigma(I_0)/n_0)]$, where n and n_0 are the numbers of I and I_0 pixels, respectively. This protocol averages over any fine-scale heterogeneity and provides XANES spectra that are representative of the bulk IOM with very high signal to noise. It is noted that no significant fine-scale chemical heterogeneity was obvious in any of the hyperspectral data sets.

In this study, we are primarily concerned with spectral differences. Consequently, the spectra were normalized to the C-XANES intensity at 340 eV where EXAFS oscillations should be minimal and the atomic C absorption dominates.

RESULTS

Elemental and Isotopic Compositions

Elemental and isotopic analyses of the IOM from the four lithologies are given in Table 1. Averages were previously reported by Herd et al. (2011). For three of the lithologies, two separate aliquots were analyzed. Analyses of the two aliquots agree very well, with the exception of 5b. The C yield from the second aliquot of 5b was lower than the first aliquot and the other samples, and the H/C ratio was lower in the first 5b aliquot compared with the second. Otherwise, there is good agreement between the two aliquots of 5b. The low C yield of 5b(2) could simply reflect sample heterogeneity or an analytical artifact.

Except for 5b(2), the bulk IOM C contents and C yields were remarkably similar and close to the approximately 2 wt% of the lithologies that were examined in the first Tagish Lake studies (Grady et al. 2002). The N/C ratios and $\delta^{15}N$ and $\delta^{13}C$ values of all the samples are also very similar to each other. In terms of N/C ratios and $\delta^{15}N$ values, the Tagish Lake lithologies all form a tight cluster that is distinct from other CI-2 chondrites (Fig. 1a). However, there are striking, correlated differences ($r^2 = 0.97$) between H/C ratios and δD values (Fig. 1b). The IOM in lithology 5b has an H/C ratio that is similar to CI-CM-CR IOM and a δD value that is intermediate between typical CM and CR chondrites (Fig. 1b).

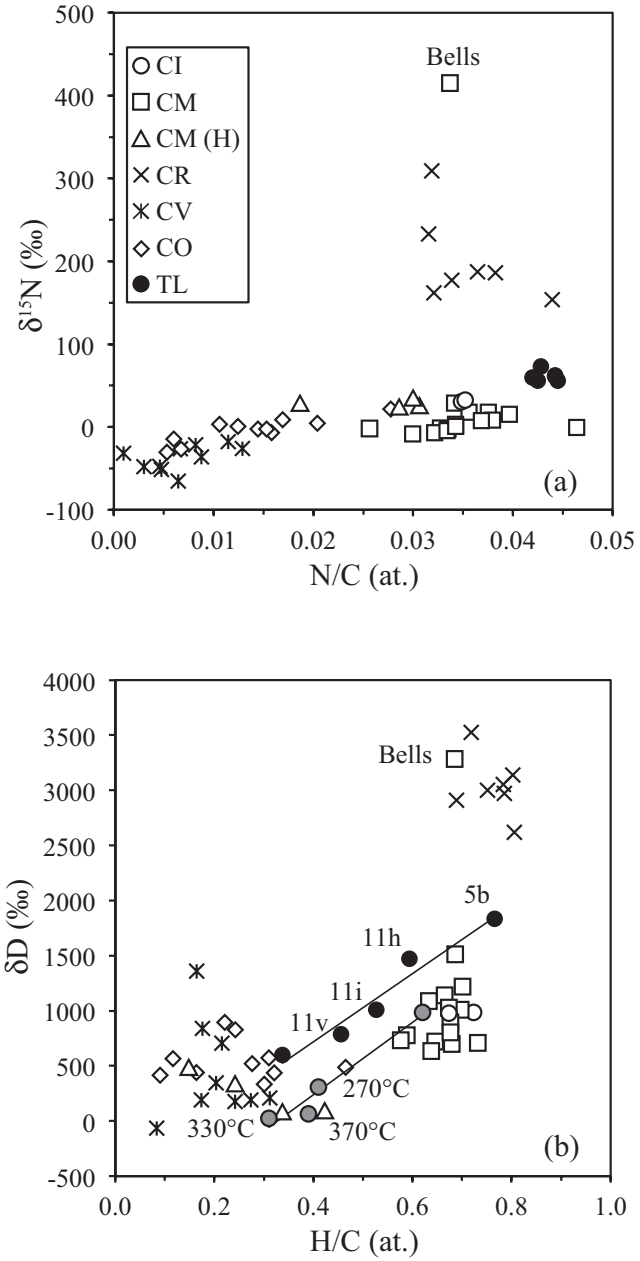

Fig. 1. Comparison of the IOM N and H elemental and isotopic compositions in Tagish Lake (Table 1) and other carbonaceous chondrites (Alexander et al. 2007, 2010): (a) $\delta^{15}N$ versus N/C (at) and (b) δD versus H/C. The gray filled circles in (b) are from hydrothermal experiments conducted on Murchison IOM by Oba and Naraoka (2009)—the run durations were 3 days and the run temperatures are indicated on the plot. The lines in (b) are best fits to the Tagish Lake IOM and the hydrothermal experiments data.

The IOM accounts for roughly half of the C and N in the bulk samples (Tables 1 and 2), but only 10–12% of the H. The C isotopic composition of the total bulk C is significantly more positive than that of the IOM. By difference, the residual carbonaceous material, composed of leachable organic matter and carbonate, must be significantly heavier than the bulk samples and IOM (Table 2). The differences among the bulk, residual, and IOM N isotopic compositions are considerably smaller, but still statistically different.

^{13}C and ^{1}H NMR Spectroscopy

The ^{13}C VACP MAS NMR spectra of the IOM residues isolated from the four Tagish Lake lithologies have been normalized, so that the total areas under the curves are the same (Fig. 2). The very broad resonances, and at least some intensity spanning the entire ^{13}C chemical shift range (approximately 0–240 ppm), demonstrates that the molecular structures of all the IOM samples are extremely complex. The small peaks centered at roughly −20 ppm and 280 ppm are spinning side bands that arise from incomplete MAS averaging of the aromatic chemical shielding anisotropy.

Notwithstanding this chemical complexity, ^{13}C in various functional groups resonates in specific frequency regions of the ^{13}C spectrum. For example, in the lowest frequency region of the spectrum, CH_3, CH_2, and CH resonate from 0 ppm up to 50 ppm. The clearly defined peak at approximately 26 ppm (Fig. 2) has been shown previously to be CH_3 through interrupted decoupling experiments (Cody et al. 2002). The signal in the spectral range from 50 to 95 ppm corresponds to sp^3-hybridized (aliphatic) C bonded to O, as in the case of alcohols and ethers. The intensity spanning 95 ppm up to 240 ppm is due to sp^2-hybridized carbon: aromatic and olefinic C contributes intensity from 95 up to 145 ppm; enol C (e.g., phenol) produces intensity in the spectral range from 145 up to 160 ppm; and carbonyl C (e.g., ketone and carboxyl) creates intensity in the range from 160 to approximately 220 ppm.

There are significant differences in molecular structure going from the IOM isolated from lithology 5b to that from lithology 11v (Fig. 2), with a reduction in the abundance of sp^3-bonded C, both CH_x (e.g., methyl, methylene, and methine) and CH_xO (e.g., ether and alcohol), relative to aromatic C. This trend is very similar to that observed in an earlier cross group NMR study of IOM derived from CR, CI, CM chondrites and a different sample of Tagish Lake (Cody and Alexander 2005).

While the aromatic content increases considerably moving from lithology 5b to 11v, the frequency of this absorption remains close to 130 ppm. This is significant, because IOM derived from thermally metamorphosed chondrites, e.g., Allende (CV 3.6), exhibits large negative paramagnetic shifts in its aromatic resonance to a

Table 2. The bulk H, C, and N abundances and isotopic compositions of three of the four Tagish Lake lithologies (Alexander et al. 2012), and the residual composition after subtracting the IOM (Table 1).

	H[a](wt%)	C (wt%)	N (wt%)	δD^1 (‰)	$\delta^{13}C$ (‰)	$\delta^{15}N$ (‰)
Bulks						
11i	0.738 ± 0.009	3.95	0.17	542 ± 9	14.0	59.7
11h	0.872 ± 0.004	4.13	0.19	557 ± 6	9.4	62.6
5b	0.945 ± 0.003	4.11	0.24	508 ± 4	10.1	76.2
Bulks-IOM						
11i	0.66	2.13	0.085	490	37.3	66.7
11h	0.77	2.28	0.099	448	28.8	67.8
5b[b]	0.83	2.25	0.146	317	30.4	86.1

[a]The uncertainties are the 1σ of two analyses.
[b]Only the first 5b IOM analysis in Table 1 was used.

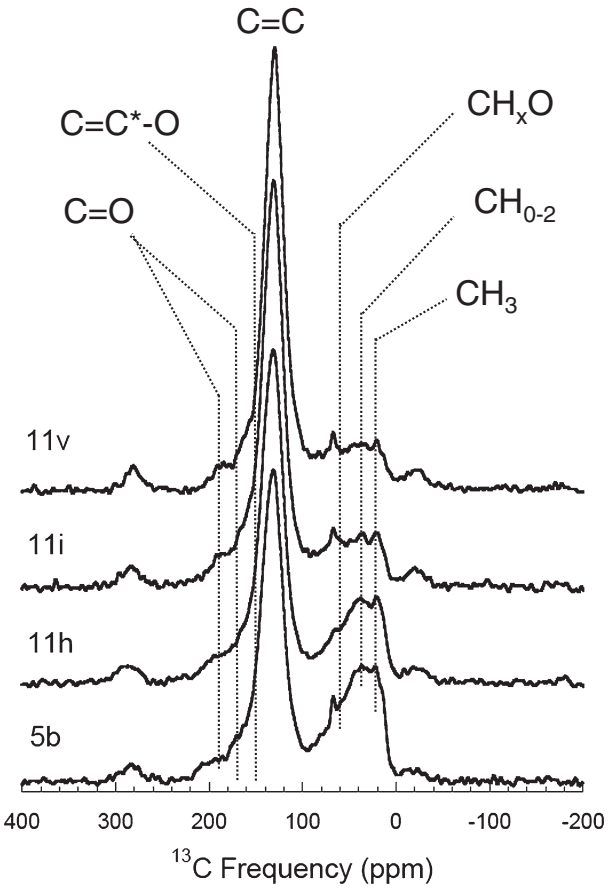

Fig. 2. ^{13}C VACP MAS NMR spectra of Tagish Lake IOM isolated from lithologies 5b, 11h, 11i, and 11v (bottom to top, respectively). The ^{13}C spectrum reports the distribution of C into different electronic environments. At the first level, the ^{13}C NMR spectrum separates sp^3 C from sp^2 C in frequency, 0–100 ppm and 100–220 ppm, respectively. Note that the intensities, between −30 ppm and 0 ppm, and 280 ppm and 320 ppm are due to incomplete averaging of the chemical shielding anisotropy of aromatic C (130 ppm) resulting in spinning sidebands. Specific functional groups in the spectra are as follows: CH_3 (0–28 ppm), CH_2-CH (28–50 ppm), CH_xO (50–95 ppm), aryl and olefinic C (95–145 ppm), enol C (145–160 ppm), carbonyl C (160–220 ppm).

frequency of approximately 115 ppm, consistent with the thermally induced formation of graphene domains (Cody et al. 2008b). The lack of such a paramagnetic shift in the most aromatic-rich Tagish Lake lithology 11v indicates that whatever the process that transformed the IOM, the process was distinct from the long-term, high-temperature metamorphism that thermally metamorphosed type 3 chondrites were subjected to.

DP ^1H MAS NMR also reveals considerable differences in molecular structure (Fig. 3). The chemical shift range for ^1H is much narrower than that for ^{13}C, owing to the much lower electron density surrounding the ^1H nucleus. Also, as ^1H is an abundant nucleon, ^1H-^1H dipolar coupling in the sample leads to residual line broadening in spite of the relatively fast MAS employed here. One can readily distinguish aliphatic ^1H from aromatic/olefinic ^1H, with resonances that range from approximately −30 ppm to 3.5 ppm and from 6 ppm up to approximately 30 ppm, respectively. The extension of signal down to −30 ppm and up to 30 ppm is entirely due to residual dipolar coupling. Given that the ^{13}C spectra (Fig. 2) reveal significant intensity corresponding to CH_xO moieties, it is expected that CH_xO H should also contribute some intensity to the ^1H NMR spectrum in the region spanning from 3.5 to 6 ppm.

The NMR spectra were integrated to calculate quantitative functional group abundances. Given that both the ^{13}C and the ^1H NMR spectra are very broad, fitting of the spectra with multiple, overlapping peaks is ill advised as the choice of peak shape (e.g., Lorenztian, Gaussian, or mixed), peak widths, and number of peaks is unconstrained. A less subjective approach to fitting such broad spectra is to directly integrate the spectra using the established ranges of chemical shifts that correspond to different electronic environments (Pretsch et al. 2000). Such integrations were performed for both the ^1H and the ^{13}C spectra using the spectral ranges defined above (Table 3).

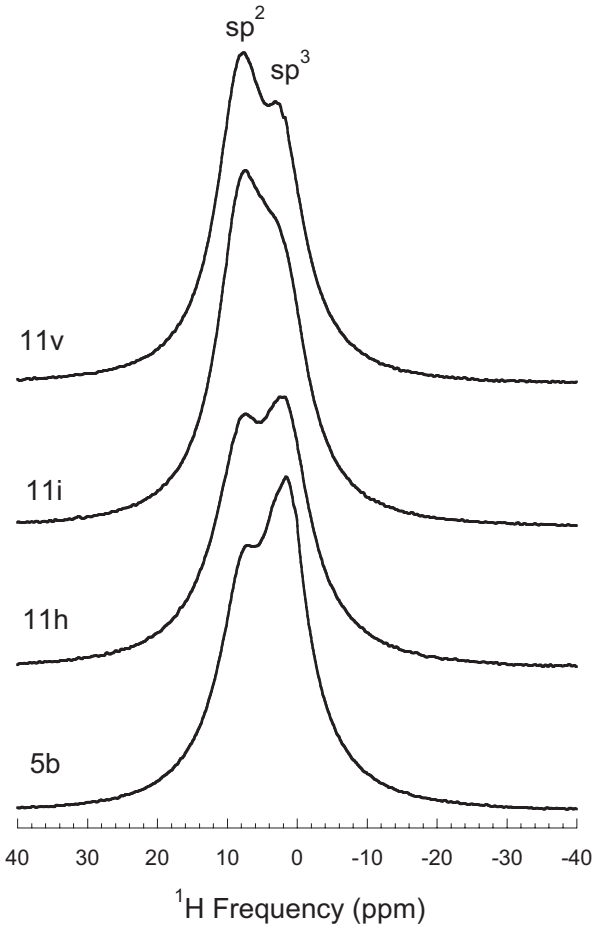

Fig. 3. ^{1}H DPMAS NMR spectra of Tagish Lake IOM isolated from lithologies 5b, 11h, 11i, and 11v (bottom to top, respectively). The ^{1}H spectrum reports the distribution of H into different electronic environments. The most prominent features are H bonded to sp^3 and sp^2 C.

Table 3. Molecular structural parameters derived from ^{1}H and ^{13}C solid-state NMR.

Molecular Parameters	TL-5b	TL-11h	TL-11i	TL-11v
^{13}C NMR				
Fraction CH_3	9.1	7.7	4.6	4.4
Fraction CH_2 + CH	13.7	10.3	6.2	5.8
Fraction CH_xO	14.1	10.6	10.1	9.8
Fraction C=C[a]	46.1	51.6	59.1	64.5
Fraction C=C–O[a]	8.6	9.7	9.9	8.4
Fraction C=O	8.4	10.0	10.1	7.1
Fraction aromatic C[a]	0.55	0.61	0.69	0.73
^{1}H NMR				
H in CHx (x = 1,2 & 3)	47.9	43.4	36.6	35.9
H in CHxO (x = 1 & 2)	13.8	13.2	15.2	14.2
H aromatic/olefinic	38.2	43.4	48.2	49.9
Determined Parameters				
% aromatic substitution[b]	49.9	58.0	64.4	69.9
X in aliphatic CH_x[c]	1.2	1.2	1.3	1.1

[a]Includes contributions from spinning sidebands.
[b]Determined from the proportion of aromatic H and C, and the atomic H/C.
[c]Determined from the proportion of aliphatic H and C, and the atomic H/C.

Micro-FTIR Spectroscopy

The IR absorption spectra of Tagish Lake IOM revealed organic functional groups that were identified by their characteristic vibrational frequencies. The spectra were divided into two regions (3800–2700 cm^{-1} and 1900–800 cm^{-1}), and the steep baseline produced by scattering was corrected for by subtracting a linear fit to the baselines of each region; the background-subtracted spectra are shown in Fig. 4. The identities and frequencies of the characteristic IR absorption bands are summarized in Table 4.

In the high-frequency region of the IR spectra (Fig. 4a), all of the spectra exhibit a broad band centered at approximately 3400 cm^{-1} due to O–H stretching modes (including alcohol, carboxyl, and H bonded water), a weak 3067 cm^{-1} band due to aromatic C–H stretching modes, an intense triplet at around 2900 cm^{-1} due to aliphatic C–H stretching modes (including 2960 cm^{-1} due to CH_3 asymmetric stretching, 2925 cm^{-1} due to CH_2 asymmetric stretching, and approximately 2860 due to symmetric stretching of CH_3 and CH_2). In the so-called "finger print" region of the IR spectrum (Fig. 4b), an intense 1703 cm^{-1} band was observed due to carboxyl/ester C=O stretching modes, an intense 1588 cm^{-1} band due to aromatic C=C stretching modes, and fine structure vibrational modes in the range of 1500 cm^{-1} to 1000 cm^{-1} (including 1450 and 1375 cm^{-1} due to aliphatic C–H bending and around 1220 cm^{-1} due to an aromatic skeletal mode) (Fig. 4b). Some spectra exhibit weak 1118, 1080, and 1035 cm^{-1} bands that are reasonably assigned to C–O stretching modes, indicative of the presence of alcohols and/or ethers.

The ratios of the peak areas of several of the most prominent peaks (Table 5) are plotted against one another in Fig. 5 and compared to those for IOM from Grosvenor Mountain (GRO) 95577 (CR1), Elephant Moraine (EET) 92042 (CR2), Murchison, Semarkona, (LL3.00), Allan Hills (ALH) 77307 (CO3.0), Kaba (CV3.1), Allende (CV3), and Yamato (Y-) 86720 (CM heated) (Kebukawa et al. 2011).

The (CH_2+CH_3)/aro-CH and (CH_2+CH_3)/C=C ratios are positively correlated, with the ratios decreasing in the order 5b>11h > 11i>11v≈old (Fig. 5a). The IOM from Murchison, GRO 95577, Y-86720, and Semarkona also fall on this trend. The larger error bars for Murchison and GRO 95577 reflect the poorer quality of the previously acquired spectra. Poorer

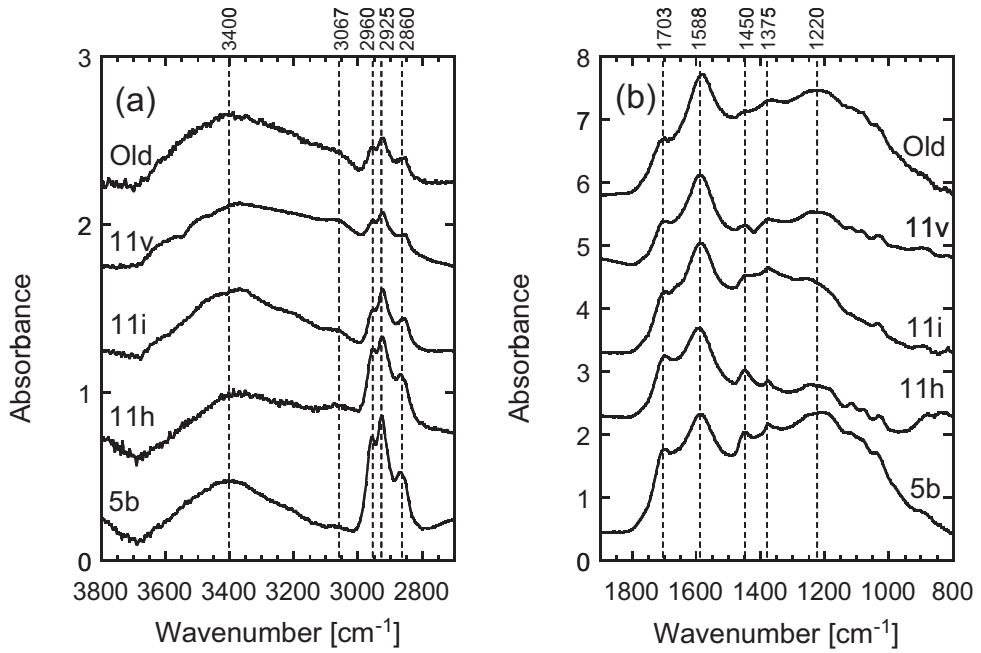

Fig. 4. Fourier transform infrared (FTIR) spectra of Tagish Lake IOM isolated from lithologies 5b, 11h, 11i, and 11v (bottom to top, respectively). The "old" spectrum is for a previously studied Tagish Lake IOM sample (Kebukawa et al. 2011). The absorbance is in arbitrary units. For comparison, the spectra have been offset from one another. The intensities of all spectra have also been normalized to the peak heights of the aromatic C=C bands at approximately 1590 cm^{-1} relative to lines drawn between points at 1800 cm^{-1} and 1500 cm^{-1}. (a) The high frequency region of the FTIR spectra that highlights X-H stretching vibrational modes. The broad absorption spanning 3700–3000 wave numbers (cm^{-1}) correspond to O–H stretching modes, the small peak at approximately 3070 cm^{-1} corresponds to C–H stretching (aromatic), the triplet peaks at 2960, 2925, and 2860 cm^{-1} correspond to aliphatic (methyl and methylene) stretching symmetric and asymmetric C–H stretching vibrations. (b) The "finger print" region of the FTIR spectrum where carbonyl stretching is prominent at approximately 1700 cm^{-1}, aromatic C=C stretching is obvious at approximately 1590 cm^{-1}, and various other more complex vibrational resonances contribute to intensity below 1500 cm^{-1}.

quality is also the reason for there being no detection of the weak aromatic C–H feature in some of the other previously acquired spectra. Both the C=O/C=C and the (CH_2+CH_3)/C=C ratios also decrease in the order 5b>11h > 11i>11v≈old in a linearly correlated fashion (Fig. 5b). The IOM from Murchison and GRO 95577 plot on an extension of this trend, while the IOM from EET 92042 and Semarkona are offset to slightly higher C=O/C=C ratios and the heated meteorites Allende, ALH 77307, and Kaba are offset to lower C=O/C=C ratios. The CH_2/CH_3 ratios in the IOM increase in the order 5b<11h < 11i<11v≈old, and are roughly inversely correlated with the (CH_2+CH_3)/C=C ratios (Fig. 5c). However, when the other meteorites are included, the relationship between the two ratios is more complex, and there is no clear distinction between the primitive and heated samples.

Carbon XANES

Absorption in the C-XANES region provides information about the bonding environments present and is complementary to information obtained by ^{13}C solid-state NMR. Figure 6 compares the C-XANES spectra of IOM from lithologies 5b and 11v. Interestingly, while comparison of the ^{13}C solid-state NMR spectra of these IOM samples (Fig. 2) reveals considerable differences in the abundance of different functional groups, the C-XANES spectra are, superficially, very similar. One observes apparently similar functional groups (Fig. 6) at nearly the same intensities. Given the increase in aromatic C evident in the ^{13}C solid-state NMR spectra (Fig. 2), one might expect the intensity of aromatic 1s-π* absorption (A, at 285 eV, Fig. 6) in the C-XANES spectrum of the 11v IOM to be significantly higher than that observed for 5b IOM. Rather, what is observed is a broadening of the 1s-π* region. Such broadening is best explained by the presence of more highly condensed aromatic clusters in the IOM from lithology 11v compared with that in lithology 5b, i.e., the C-XANES data indicate a difference in the aromatic structures between 5b and 11v.

It is also notable that in the case of IOM derived from thermally metamorphosed type 3 chondrites, e.g.,

Table 4. Peaks observed with FTIR and their possible assignments, after Socrates (2001).

Peak position (cm^{-1})	Vibrational mode	Functional group
3400	O–H stretch	Alcohol, carboxyl, water
3067	C–H stretch	Aromatic CH
2960	C–H asymmetric stretch	Aliphatic CH_3
2925	C–H asymmetric stretch	Aliphatic CH_2
2860	C–H symmetric stretch	Aliphatic CH_3 and CH_2
1703	C=O stretch	
1588	C=C stretch	Aromatic
1450	C–H asymmetric bend	Aliphatic CH_3
1375	C–H symmetric bend	Aliphatic CH_3
1220	Aromatic skeletal	
1118, 1080, 1035	C–O stretch?	

Allende, a sharp peak at 291.7 eV corresponding to a 1s-σ* exciton is observed (Cody et al. 2008b). This is not the case for the heated CM Y-86720. The presence of the exciton is a signature of the presence of graphene that formed during thermal metamorphism over an extended period of time (millions of years). Apparently, Y-86720 was heated for a much shorter period of time, perhaps by an impact. In the case of IOM in lithology 11v, which appears to be the most modified of the IOM from the four Tagish Lake lithologies, there is no indication of the 1s-σ* exciton (peak F, Fig. 6). The lack of an exciton is to be expected given the lack of any paramagnetic shift of the aromatic peak in the ^{13}C NMR data (Fig. 2), and is consistent with previous XANES studies of Tagish Lake IOM (Cody et al. 2008b). If the IOM from 11v was heated, the heating was at modest temperatures and/or for short times.

To more clearly reveal the differences in the C-XANES spectra of IOM from lithologies 5b and 11v, spectral subtraction was performed after both spectra were baseline corrected and scaled, so that their absorption intensities at 340 eV were identical. The difference spectrum (5b-11v) is presented in Fig. 7. The higher relative aromatic C content of 11v is clearly evident from the negative peak centered at 285 eV (feature 1). The more abundant CH_x and CH_xO C in 5b is clearly evident in the positive peak (feature 2) in the energy range 287–290 eV. The broad negative peaks spanning 300–340 eV are not XANES features, but manifestations of photoelectron scattering, i.e., EXAFS features. As the local electronic structure becomes more ordered, EXAFS features become more pronounced. The presence of such features in the negative region of Fig. 7 reflects the proportional increase in both the aromatic C and its ordering (i.e., more perfectly hexagonal bonding) in 11v. This increased EXAFS intensity reflects more condensed aromatic structures that provide more coherent photoelectron scattering.

DISCUSSION

The petrology, mineralogy, and bulk O isotopes all indicate that the four Tagish Lake lithologies are from the same parent body, and that their differences reflect variations in the degree of aqueous alteration (Herd et al. 2011, 2012; Blinova et al. 2014b). Hence, the correlated variations in IOM H/C ratios; δD values;

Table 5. The intensity ratios of absorption peaks identified in FTIR spectra. The errors are all 1σ.

		N[b]	C=O/C=C	Ali-CH/Aro-CH[c]	Ali-CH/C=C[c]	CH_2/CH_3	CH_2/CH_3[d]
Tagish Lake[a]	Old	30	0.49 ± 0.15	6.5 ± 3.0	0.10 ± 0.04	1.89 ± 0.60	2.64 ± 0.84
Tagish Lake	11v	27	0.44 ± 0.08	5.5 ± 2.4	0.09 ± 0.05	1.70 ± 0.28	2.37 ± 0.40
Tagish Lake	11i	24	0.63 ± 0.11	9.6 ± 5.5	0.16 ± 0.05	1.40 ± 0.15	1.96 ± 0.21
Tagish Lake	11h	18	0.70 ± 0.07	23.8 ± 4.6	0.30 ± 0.04	1.23 ± 0.04	1.72 ± 0.06
Tagish Lake	5b	19	0.88 ± 0.13	29.9 ± 21.5	0.38 ± 0.08	1.17 ± 0.09	1.63 ± 0.13
GRO 95577[a]	CR1		1.16 ± 0.10	53.0 ± 20.3	0.47 ± 0.03	1.46 ± 0.05	2.04 ± 0.08
EET 92042[a]	CR2		1.13 ± 0.07	–	0.34 ± 0.02	1.22 ± 0.07	1.70 ± 0.10
Murchison[a]	CM2		0.96 ± 0.08	51.5 ± 15.2	0.52 ± 0.03	1.51 ± 0.05	2.12 ± 0.07
Y-86720[a]	CM2 (H)		–	9.3 ± 2.1	0.19 ± 0.02	1.53 ± 0.17	2.14 ± 0.24
Semarkona[a]	LL3.00		0.86 ± 0.10	4.9 ± 0.4	0.13 ± 0.01	1.62 ± 0.06	2.27 ± 0.08
ALH 77307[a]	CO3.0		0.37 ± 0.11	–	0.14 ± 0.03	1.99 ± 0.55	2.79 ± 0.77
Kaba[a]	CV3.1		0.37 ± 0.04	–	0.17 ± 0.01	1.90 ± 0.17	2.66 ± 0.23
Allende[a]	CV3 > 3.6		0.22 ± 0.09	–	0.10 ± 0.02	2.67 ± 1.08	3.74 ± 1.51

[a]Data from Kebukawa et al. (2011).
[b]Number of spectra.
[c]Ali-CH=(CH_2+CH_3), Aro-CH = aromatic C–H.
[d]The molecular ratios were calculated using $N_{CH_2}/N_{CH_3} = 1.4x(Abs_{CH_2})/(Abs_{CH_3})$.

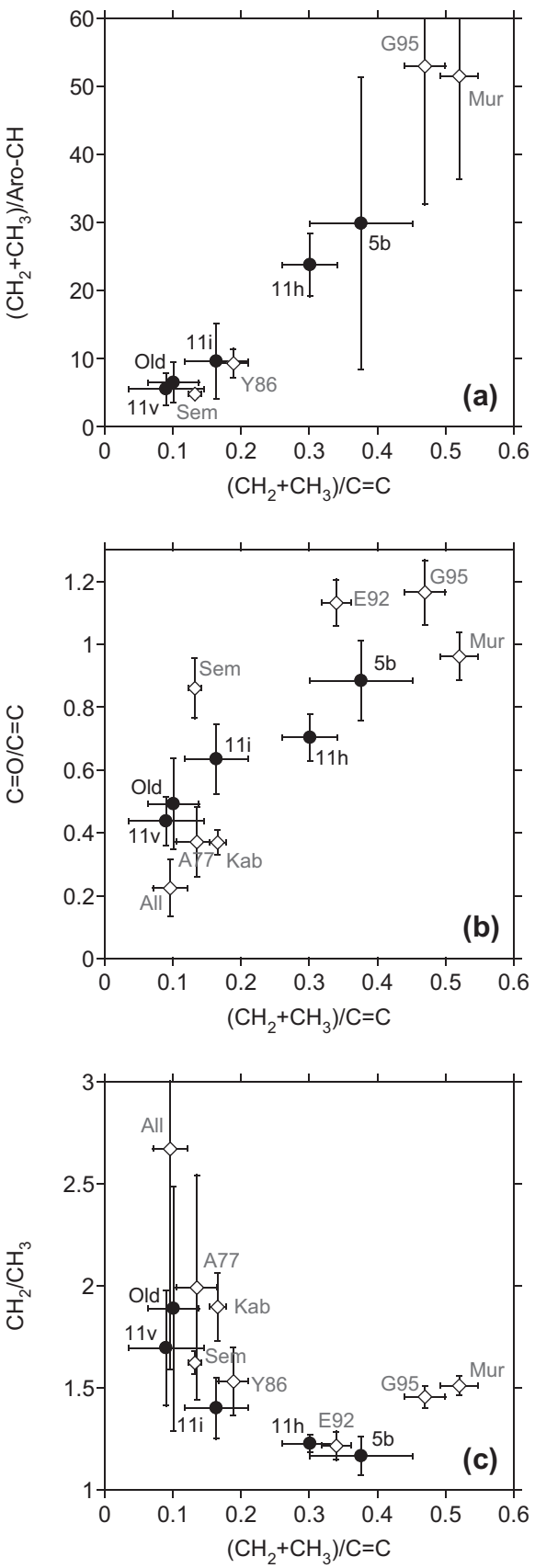

Fig. 5. Trends in the relative concentrations of organic functional groups determined by FTIR for IOM from the four Tagish Lake lithologies and a previously studied Tagish Lake IOM sample (Kebukawa et al. 2011) (Table 5). For comparison, data for type 1 (GRO 95577 or G95, CR1) and type 2 (Murchison or Mur, CM2, and EET 92042 or E92, CR2) IOM are included, as are data for thermally altered IOM from Allende (All, a CV3.6), Y-86720 (Y86, a thermally altered CM), Semarkona (Sem, LL3.0), ALHA77307 (A77, CO3.0), and Kaba (Kab, CV3.1). (a) The total aliphatic C–H stretching (CH_2 and CH_3 at 2950 cm^{-1}) to aromatic stretching (C=C, at 1600 cm^{-1}) intensity ratio versus total aliphatic C–H stretching to the aromatic CH stretching (aro-CH, at 3070 cm^{-1}) intensity ratio. (b) The carbonyl (C=O, at 1715 cm^{-1}) stretching to C=C intensity ratio versus the $(CH_2+CH_3)/C=C$ intensity ratio. Among the Tagish Lake IOM samples, the ratios correlate positively. (c) The CH_2/CH_3 intensity ratio versus the $(CH_2+CH_3)/C=C$ ratio.

and NMR, XANES, and IR spectra must then reflect parent body modification in a common IOM. As this modification correlates with petrologic estimates of the extent of aqueous alteration (Herd et al. 2011), presumably some form of hydrothermal process was responsible for the modification. Below, we explore what constraints can be placed on the transformation process based first on the elemental and isotopic analyses, and then on the functional group information gleaned from the NMR, XANES, and IR measurements.

IOM Abundances and Elemental and Isotopic Compositions

The variation in IOM H/C ratios implies increasing aromaticity in the IOM with increasing degree of alteration, which is borne out by the NMR and IR spectroscopy (Figs. 3–5). Despite the dramatic variations in H/C ratio and aromaticity, the IOM C yields in the bulk lithologies and IOM N/C ratios do not vary significantly (Table 1).

If, as discussed above, we assume that the IOM abundance obtained for sample 5b(2) is anomalously low, the mean IOM abundances in the four lithologies vary by only a few percent. Typically, reported IOM abundances for a given chondrite vary by 10–20% (Alexander et al. 2007). The IOM is found exclusively in the matrix. Presumably, the variations in reported IOM abundances reflect variations in the matrix abundances of the analyzed samples, as well as differences in the isolation techniques. The high matrix content (approximately 80 vol%) of Tagish Lake will have reduced the chances of variations in IOM yields due to sample heterogeneity. This and the use of a single isolation technique will have contributed to the reproducibility of the IOM abundance determinations reported here.

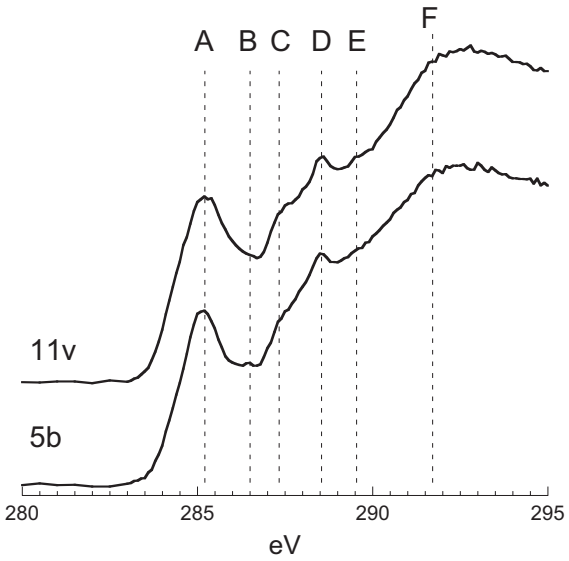

Fig. 6. Carbon-XANES spectroscopy of IOM from Tagish Lake lithologies 5b (bottom) and 11v (top); the *Y*-axis is absorbance in arbitrary units and the spectra have been offset from one another to facilitate their comparison. Absorption fine structure corresponds to C (1s) photoexcitation to accessible bound states (unoccupied molecular orbitals), where (A) is the 1s-π* transition associated with aromatic/olefinic C; (B) is the 1s-π* transition associated with ene-ketone moieties; (C) is the 1s-σ*/C–H transition associated with aliphatic C; (D) is the 1s-π* transition associated with carbonyl C; (E) is the 1s-σ*/C–H transition associated with aliphatic C bonded to O, e.g., alcohol and ether; and (F) the spectral position where the very sharp 1s- σ* transition is expected if graphene were present, a signature of high-temperature, long-duration metamorphism in type 3 chondrites (Cody et al. 2008a, 2008b).

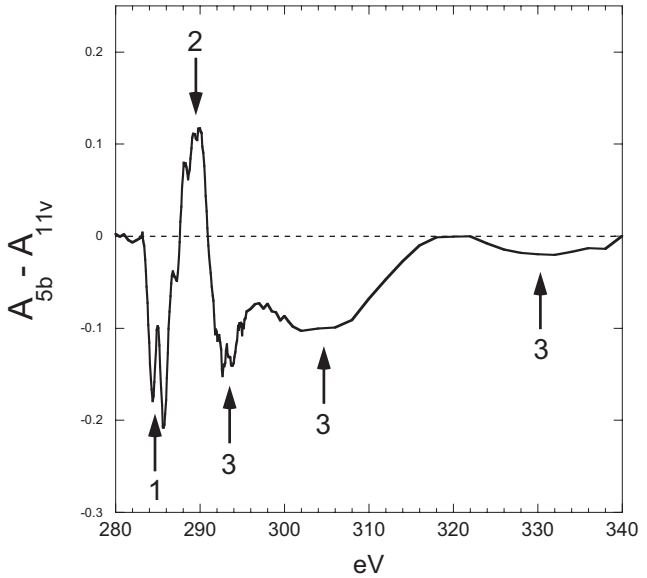

Fig. 7. Carbon-XANES difference spectrum, 11v IOM subtracted from 5b IOM revealing the differences in electronic structure between the two residues. Negative features correspond to higher abundances in 11v; positive features correspond to higher abundances in 5b. (1) The negative feature at approximately 285 eV (the aromatic 1s-π* transition) indicates greater aromatic C in 11v; note that the fine structure in this feature indicates change in the aromatic electronic structure relative to 5b. (2) The positive feature spanning 287–290 eV indicates greater CH_x and CH_xO in 5b. (3) The negative features spanning from 292 eV to 330 eV are EXAFS features indicative of highly ordered aromatic C.

Alexander (2005) suggested that all chondrites had roughly CI-like IOM abundances in their matrices at the time of accretion. The bulk IOM abundances in Tagish Lake are approximately 80–90% of those in bulk CI chondrites, which is consistent with their relative matrix abundances. Alexander et al. (1998, 2007) and Cody and Alexander (2005) also argued that all chondrites accreted a common, primordial IOM whose composition and structure most closely resembled the IOM in the CR chondrites. In terms of its NMR spectrum, the IOM from lithology 5b resembles the CR IOM quite closely. However, the H and N isotopic compositions of 5b IOM are less anomalous than those measured in the CRs. If there was a common CR-like precursor, then, while the 5b IOM is the most primitive of the Tagish Lake samples, it is not pristine in an isotopic sense.

One puzzling feature of the Tagish Lake IOM is that its N/C ratio (approximately 0.042, Table 1) is consistently higher than found in IOM from almost all other primitive chondrites (Fig. 1a), including the CRs (N/C = 0.032–0.038; Alexander et al. 2007). The CM LEW 85311 does have a higher N/C ratio (0.046), but it is an anomaly. The IOM from the CR GRA 95229 also has a higher average ratio (0.044 ± 0.006), but with a large uncertainty. If the Tagish Lake IOM evolved from CR-like IOM, it must have gained N and/or lost C during parent body processing. Alternatively, the CR IOM has lost some N during parent body processing—there is a suggestion that N/C decreases with increasing extent of aqueous alteration among the CRs (Alexander et al. 2007).

The IOM accounts for slightly less than half of the bulk C and N in the lithologies (Tables 1 and 2), and approximately 5–10% of the H. The bulk of the remaining H is almost certainly in hydrated silicates, but some could still be associated with soluble and/or hydrolysable (leachable) organics that were lost during IOM extraction (Alexander et al. 2012, 2013a). The isotopic composition of the leachable N is similar to that of the IOM, whereas the $\delta^{13}C$ of the leachable C is significantly heavier than the IOM. This could be because of a sizable carbonate contribution to the bulk analyses. The Tagish Lake carbonate C isotopic composition is $\delta^{13}C \approx 68‰$ (Grady et al. 2002). Assuming an IOM-like C isotopic composition for the

other leachable carbonaceous component, roughly half of the lost C, or approximately 1 wt% C, could be in carbonate. This would be equivalent to approximately 8 wt% calcite, or 5 vol% calcite assuming a bulk density of 1.66 g mL^{-1} for Tagish Lake (Zolensky et al. 2002). A carbonate C abundance of approximately 1 wt% is consistent with the estimated carbonate C abundance of 1.29 wt% obtained by Grady et al. (2002). However, their small Tagish Lake sample had a bulk C content of 5.8 wt% and a $\delta^{13}C = 24.4‰$. Both the bulk C content and the isotopic composition are significantly higher than obtained for the three lithologies analyzed by us (Table 2), suggesting that, as suspected by Grady et al. (2002), their sample was not truly representative—both the IOM content and the proportion of C in carbonate are higher. This interpretation is supported by the work of Pearson et al. (2006) who found the bulk C content and isotopic composition for Tagish Lake to be 4.25 ± 0.21 wt% and $\delta^{13}C = 12.7 \pm 0.4‰$, respectively, which are very similar to those obtained here for the three lithologies listed in Table 2. It seems possible that there are organics in Tagish Lake that, on average, have significantly heavier C isotopic compositions than the bulk IOM, for instance as a result of exchange or reaction with carbonate in solution (Herd et al. 2011). Thus, at least half and possibly significantly more of the leachable C are organic.

The simplest explanation of the relatively constant abundances of IOM C and N in the four lithologies is that aliphatic material was converted to aromatic material. This would have involved the loss of H, but apparently was achieved without changing the concentrations of either C or N. The linear correlation between H/C and δD values (Fig. 1b) suggests that, in the process of the aliphatic-aromatic conversion, either IOM H isotopically exchanged with less D-rich water or there was preferential loss of a D-rich component from the IOM. The fact that N was not lost during this process indicates that either it was initially entirely contained in the aromatic component (Oba and Naraoka 2009) or, if some fraction was in the aliphatic material, it was quantitatively retained. In coals, N/C ratios also tend to stay fairly constant during maturation, at least until H/C ratios fall below about 0.3 (Van Krevelen 1993; Jiang et al. 2002).

Finally, petrologically the extent of aqueous alteration appears to increase from lithologies 5b to 11h to 11i (Herd et al. 2011). Thus, it is puzzling that the bulk H contents of these lithologies, even after IOM subtraction, decrease going from 5b to 11i (Table 2). The most likely explanation of this is that there has been some dehydration of 11h and 11i. Mass fractionation associated with the water loss could potentially help explain the higher bulk $\delta^{18}O$ values of 11h and 11i compared with 5b (Herd et al. 2012). There is no evidence that lithologies 11h and 11i have been shock heated. At present, how and when the dehydration may have occurred remains unresolved.

Functional Group Chemistry

Fitting of the ^{1}H and ^{13}C NMR data, subject to the constraints of known chemical shift ranges for organic functional groups, provides a quantitative measure of the distributions of IOM functional groups. Combining these data with the bulk IOM H/C ratios (Table 1) allows one to extract additional molecular structural information (Table 3). For example, not only does the fraction of aromatic C increase from 5b to 11v but also the derived average degree of aromatic substitution progressively increases with increasing aromaticity (or decreased H/C) from 49.9% aromatic C in lithology 5b IOM up to 69.9% aromatic C in lithology 11v IOM, a substantial difference. This increase in substitution, combined with the loss of all other functional groups, indicates that aromatic condensation reactions dominated the molecular transformations from 5b to 11v. In other words, smaller ring systems condensed to form larger ring systems, losing aromatic H in the process. As noted above, increased aromatic condensation is supported by the C-XANES data that reveals broadening of the 1s-π* manifold of states (Figs. 6 and 7).

One can also determine the average H content of the aliphatic moieties from the NMR data (Cody et al. 2002), e.g., CH_x, where $X = 3$ corresponds to methyl, $X = 2$ corresponds to methylene, and $X = 1$ corresponds to methine. For the IOM from all of the lithologies, both the aliphatic and the oxygenated aliphatic (sp^3 hybridized) C groups have low values of X (1.1–1.3), indicating highly branched aliphatic structures that require considerable methine and, possibly, quaternary C. Similarly low values of X were found in earlier analysis of Tagish Lake IOM, as well as for primitive IOM from other meteorite groups (Cody and Alexander 2005). The presence of highly branched aliphatic material is also consistent with CH_2/CH_3 ratios that are greater than unity as determined by IR spectroscopy (Table 5). Combining the NMR and IR data and assuming $X = 1.2$, the average for all lithologies (Table 3), the proportions of CH, CH_2, and CH_3 in the aliphatic material of the IOM in lithologies 5b and 11h are roughly 0.85:0.09:0.05. It is interesting that while the IOM H/C, aromaticity, and aromatic condensation all increase from lithology 5b to lithology 11v, the structure of the aliphatic moieties, as judged from the X values, does not change significantly. The FTIR results

(Table 5) indicate that there is an increase in the CH_2/CH_3 ratios with increasing aromaticity, albeit with relatively large errors, but this would require only slight decreases in the CH abundances to maintain constant values of X (e.g., proportions of 0.84:0.11:0.04 for the old Tagish Lake sample). There is significant O functionality in the aliphatic material that will drive down the aliphatic H/C ratio. Nevertheless, it is clear that the aliphatic material must be heavily branched, so much so that we cannot rule out that quaternary C is a component of the aliphatic material. If there is significant quaternary C in the IOM, this suggests an intriguing potential link between the IOM and the nanodiamonds that are known to make up a few percent of the C in the residues (e.g., Grady et al. 2002; Cody and Alexander 2005).

In general, extracting quantitative functional group information from FTIR data is not possible due to uncertainties in the absorption cross sections for different organic functional groups. However, trends in IR peak ratios can reveal signatures of the molecular transformations produced by parent body processes (Kebukawa et al. 2011). The (CH_2+CH_3)/aro-CH and (CH_2+CH_3)/C=C ratios vary enormously from lithology 5b to 11v (Figs. 5a and 5b; Table 5), which is consistent with the increase in total aromatic content (Table 3). However, the linear correlation between (CH_2+CH_3)/aro-CH and (CH_2+CH_3)/C=C (Fig. 5a) implies a constant aro-CH/C=C ratio in the IOM from all the Tagish Lake lithologies. This would seem to be in conflict with the NMR and C-XANES results that indicate increasing substitution of the aromatic moieties with decreasing aliphatic C content. There is also a correlation between the (CH_2+CH_3)/C=C ratio and the ratio of integrated carbonyl C=O stretching intensity to aromatic C=C stretching intensity—these ratios decrease in order 5b > 11h > 11i > 11v (Fig. 5b; Table 5). Finally, there is the suggestion of a negative correlation between the ratio of CH_2/CH_3 stretching bands with the (CH_2+CH_3)/C=C ratio (Fig. 5c), although weak signals substantially increase the uncertainty in the derived CH_2/CH_3 ratios for the most aromatic IOM samples (11i and 11v).

Matrajt et al. (2004) reported a CH_2/CH_3 ratio of 7.3 for the bulk carbonate-rich Tagish Lake lithology from a sample collected from the lakeshore (i.e., not pristine). After refitting their spectra with our fitting protocol and using an absorption cross section ratio of 1.4, we obtained a CH_2/CH_3 ratio of 4.2. This is still significantly larger than we have obtained for the IOM in any of the Tagish Lake lithologies we have studied. The IOM properties of the carbonate-rich lithology are probably closest to those of 11v and our previously analyzed ("old") Tagish Lake sample, for which we obtained a CH_2/CH_3 ratio of 2.64 (Table 5). Our results for the "old" Tagish Lake sample and for 11v are similar to a ratio of approximately 2.4 reported by Orthous-Daunay et al. (2013) for another Tagish Lake IOM sample, after correcting for the difference in the absorption cross section ratios used here and in their study.

One possible explanation of the higher bulk meteorite CH_2/CH_3 ratio obtained by Matrajt et al. (2004) is that there is a lot more CH_2-rich material in bulk Tagish Lake than in the IOM. The total abundance of soluble organic material in Tagish Lake is a few hundred ppm (Pizzarello et al. 2001; Herd et al. 2011; Glavin et al. 2012; Hilts et al. 2014), which is much too low to influence the bulk CH_2/CH_3 ratios. Thus, if there is a difference in the CH_2/CH_3 ratios of bulk Tagish Lake and its IOM, it must be in the material that is lost during isolation of the IOM. However, comparison of bulk and IOM CH_2/CH_3 ratios shows little difference for Murchison, Bells, and Orgueil (Kebukawa et al. 2010, 2011), all of which also contain similar proportions of organic material that is lost during IOM isolation. Terrestrial contaminants can often have high CH_2/CH_3 ratios, and this seems a possible alternative explanation of the high CH_2/CH_3 ratios obtained for bulk Tagish Lake by Matrajt et al. (2004).

To place the IR data for the lithologies in a broader context, the Tagish Lake data are compared in Fig. 5 with FTIR data of primitive type 1 and 2 IOM (from Murchsion—CM2, EET 92042—CR2, and GRO 95577—CR1), a modestly thermally altered OC (Semarkona LL3.0) and two modestly thermally altered carbonaceous chondrites (ALH 77307—CO3.0, and Kaba—CV3.1), a metamorphosed CV chondrite (Allende, CV3.6), and a thermally altered CM chondrite (Y-86720). In general, the Tagish Lake IOM from lithologies 5b and 11h cluster nearer to IOM from the largely unheated IOM derived from Murchison, EET 92042, and GRO 95577, while IOM derived from thermally altered type 3 chondrites (Allende, Semarkona, ALH 77307, and Kaba) cluster more closely to IOM from Tagish Lake lithologies 11i and 11v, although, as noted above, neither the ^{13}C NMR nor the C-XANES data indicate that 11v IOM was subjected to long-term heating as severe as was Allende.

These trends in IR peak intensity ratios qualitatively reflect significant changes in Tagish Lake IOM molecular structure, with a suggestion that, moving from lithology 5b to 11v, the IOM loses carbonyl groups along with the aliphatic moieties. Furthermore, as aliphatic C is lost, CH_3 appears to decrease preferentially relative to other CH moieties. In general, these observations are consistent with what is

observed via ^{13}C and ^{1}H NMR. All the data indicate that lithology 5b IOM has the least altered molecular structure, while lithology 11v and the previously analyzed samples of Tagish Lake IOM (Pizzarello et al. 2001; Cody and Alexander 2005) have suffered significant modification leading to a highly aromatic molecular structure.

Mechanisms of IOM Modification

Overall, the combined ^{1}H DP MAS NMR, ^{13}C CPMAS NMR, C-XANES, and FTIR data reveal large and systematic differences in IOM molecular structure going from lithology 5b to 11v. The parent body process behind this change is not immediately obvious, nor can the direction of change be immediately ascertained from the chemical trends. However, if trends in terrestrial kerogen structure are used as a guide, increases in aromatic C correspond to increases in thermal maturity. Interestingly, the mineralogies and petrologies of the lithologies indicate that 5b is the least aqueously altered and lithology 11i is the most altered (Herd et al. 2011); the lithology of 11v was highly disaggregated prior to analysis and is, therefore, difficult to classify petrologically (Blinova et al. 2014b). Furthermore, it has been argued that primitive IOM from type 1 and 2 chondrites is chemically related to refractory CHON particles in comet Halley (Alexander et al. 2007), to organic particles from comet 81P/Wild 2 (Cody et al. 2008a, 2011), and to organic matter in IDPs that are thought to come from comets (e.g., Flynn et al. 2003; Busemann et al. 2006, 2009; Matrajt et al. 2012). Thus, it appears reasonable to assume that the trend in Tagish Lake IOM molecular evolution is from high H/C, high δD, and high aliphatic content to low H/C, low δD, and high aromatic content.

It was noted by Herd et al. (2011), and above, that the bulk IOM C content (wt%) does not vary significantly (<5%) among the different Tagish Lake lithologies if sample 5b(2) is ignored (Table 1). This suggests that, despite the considerable molecular structural transformation, only H was lost and that aliphatic C in the IOM was efficiently converted into aromatic C. However, in an earlier cross group IOM study (Cody and Alexander 2005), a constant aromatic C reference frame was adopted, such that the reduction in aliphatic C and increase in aromatic C was accomplished by a net loss of C, possibly through oxidative conversion of IOM ultimately to CO_2 (Cody and Alexander 2005). Some loss of C was observed in a hydrothermal experiment (300 °C for 6 days) that converted Murray IOM into material that spectroscopically resembled the most aromatic Tagish Lake IOM (Yabuta et al. 2007). A constant aromatic C reference frame would imply that any lost aliphatic material was present as side chains, rather than cross-linking moieties. The loss of cross-links would almost certainly lead to the formation of smaller, more soluble aromatic-bearing fragments.

In this study, we only have the IOM to study and have no evidence for C loss during the modification in the Tagish Lake IOM, even as hydrothermal experiments suggest that there should have been C loss and H disproportionation, at least if the modification took place at ≥300 °C (Sephton et al. 2000; Yabuta et al. 2007). Therefore, in the following discussion, we consider two endmember models as we attempt to understand the molecular transformation of the IOM: in Model 1, we assume a constant IOM C content and that only H is lost; and in Model 2, we assume a constant IOM aromatic C abundance that requires both C and H loss.

In Fig. 8, the percentages of C in various functional groups are plotted against the number of H atoms per 100 C atoms. The functional group abundances in Model 1 are those determined by NMR and given in Table 3. In Model 2, the abundances of aromatic C in the IOM from each of the lithologies are fixed to those in lithology 5b, and the abundances of the other functional groups reduced accordingly.

Assuming Model 1 (Fig. 8a), the drop in IOM H/C moving from lithologies 5b to 11i is accompanied by a significant drop in methyl and methylene + methine C, with little change moving from 11i to 11v. The drop in oxygenated sp^3 C (CH_xO) is marked from 5b to 11h, but only a small loss is observed from 11h to 11v. Carbonyl C, on the other hand, increases from 5b to 11i and then drops from 11i to 11v. The increase in carboxyl in 11h and 11i, and the relative persistence of CH_xO groups from 11h to 11v is consistent with the increase in bulk O/C from 5b to 11i, followed by a significant drop in 11v (Table 1). An increase in carbonyl C would be consistent with an oxidative mechanism, i.e., where an aqueous oxidant converts aliphatic C to carbonyl (e.g., Cody and Alexander 2005). However, as the total loss of aliphatic C far exceeds the amount of carbonyl formed (approximately 10%), the balance must be for aliphatic C to dehydrogenate to form aromatic or olefinic C. Such a reaction is also an oxidative transformation where electrons are lost as H_2. Dehydrogenation by this mechanism could lead to more polycondensed aromatic structures, consistent with the C-XANES results.

Adopting Model 2 (i.e., constant aromatic C content) changes the picture somewhat in terms of the magnitude of the functional group losses. Again, one observes a significant and progressive loss of methyl and methylene + methine C with decreasing H/C or moving

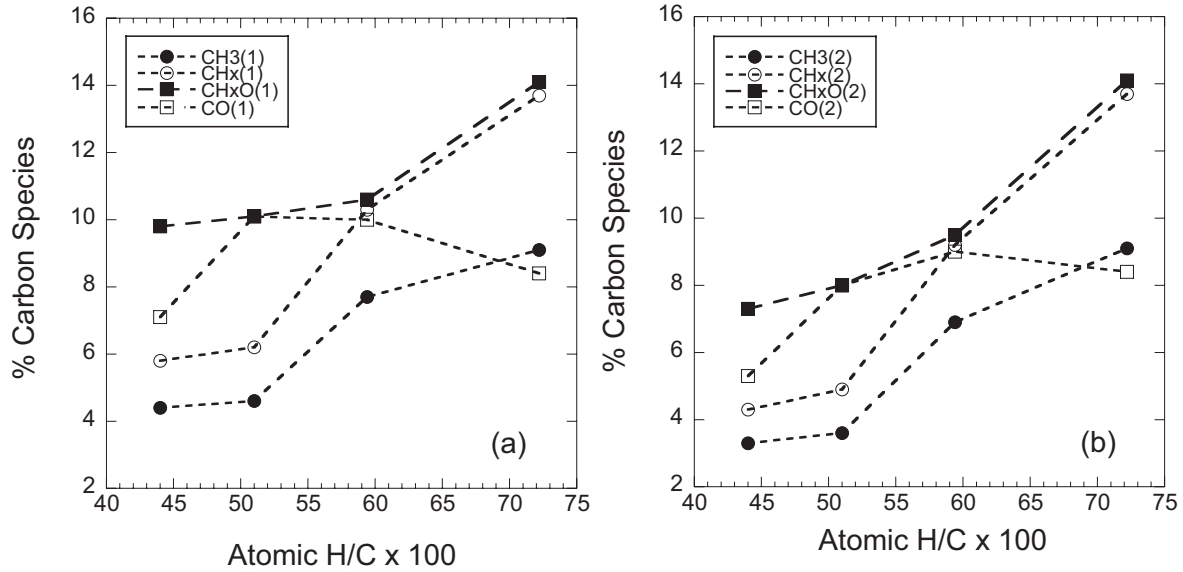

Fig. 8. Changes in C speciation moving from lithology 5b to 11v, assuming: (a) constant total C content, Model 1, and (b) constant aromatic C content, Model 2. In the case of Model 2 (b), the assumption of constant aromatic C requires a loss of approximately 25% of the original C from the IOM between 5b and 11v.

from 5b to 11v (Fig. 8b). The drop in CH_xO parallels that of methylene + methine C from 5b to 11h, but is lost at a reduced rate moving from 11h to 11v. Carbonyl C increases in concentration slightly moving from 5b to 11h, and then decreases from 11h to 11v. Model 2 presumes that all decreases in aliphatic functional groups are due to the production of low molecular weight molecules, e.g., aliphatic acids, and/or C–O–H gases. The total losses of C and H from the IOM in Model 2 are on the order of 25% and 54%, respectively. Hence, Model 2 predicts up to a 25% decrease in the bulk IOM C contents of the lithologies going from 5b to 11v. Yet, what is observed is a slight increase in IOM C content from 5b to 11v if residue 5b (2) is included, and an essentially constant C content if 5b(2) is excluded (Table 1). In both models, the final product of this transformation, 11v IOM, is oxidized relative to 5b through the disproportionate loss of H, either as pure H_2 and/or into the lower molecular weight soluble and/or gas phase products.

As required by the decrease in H/C (Table 1), significant H loss occurs in both Models 1 and 2 (39 and 54%, respectively). In the case of Model 1 (Fig. 9a), most of the H loss is derived from the transformation of methyl, methylene, and methine C to aromatic C, while a lesser amount of H is lost from the transformation of CH_xO to aromatic C. Interestingly, this does not increase the amount of aromatic H. Rather, the total aromatic H also drops moving from 5b to 11v. As discussed above, the NMR results reveal that the aliphatic moieties are highly branched, so, in principle, conversion of sp^3 C to aromatic C could occur without formation of any new aromatic H. The simplest explanation of the loss of aromatic H is through aromatic condensation reactions, e.g., the condensation of two two-benzene molecules to form biphenyl or two naphthalene molecules to form perylene. It is notable that these condensation reactions are generally thermally driven reactions.

In Model 2, the trends are largely the same, although the magnitude of the H loss is approximately 40% greater than that in Model 1. The additional H loss is due to the formation of C–O–H volatiles and small molecules that are lost from the system. In either Model 1 or 2, the pattern of H loss from all organic moieties complicates the interpretation of the variation in δD with H/C. The Tagish Lake samples show a systematic, linear decrease in δD with H/C (Fig. 1) (Herd et al. 2011) and with the fraction of aromatic C (Table 3). Superficially, this might lead one to conclude that the aliphatic C is the predominant carrier of the excess D, as has previously been inferred (e.g., Keller et al. 2004; Remusat et al. 2006). However, both of our endmember models predict that aliphatic and aromatic H is lost, so that one cannot be sure which of the organic moieties would have to be the dominant D-carrier or, for that matter, whether there actually needs to be a predominant D-carrier to explain the trend of δD versus H/C. The possibility that there is H isotope exchange with water during the structural transformations described above further complicates the interpretation of the δD versus H/C trend. Indeed, the results of

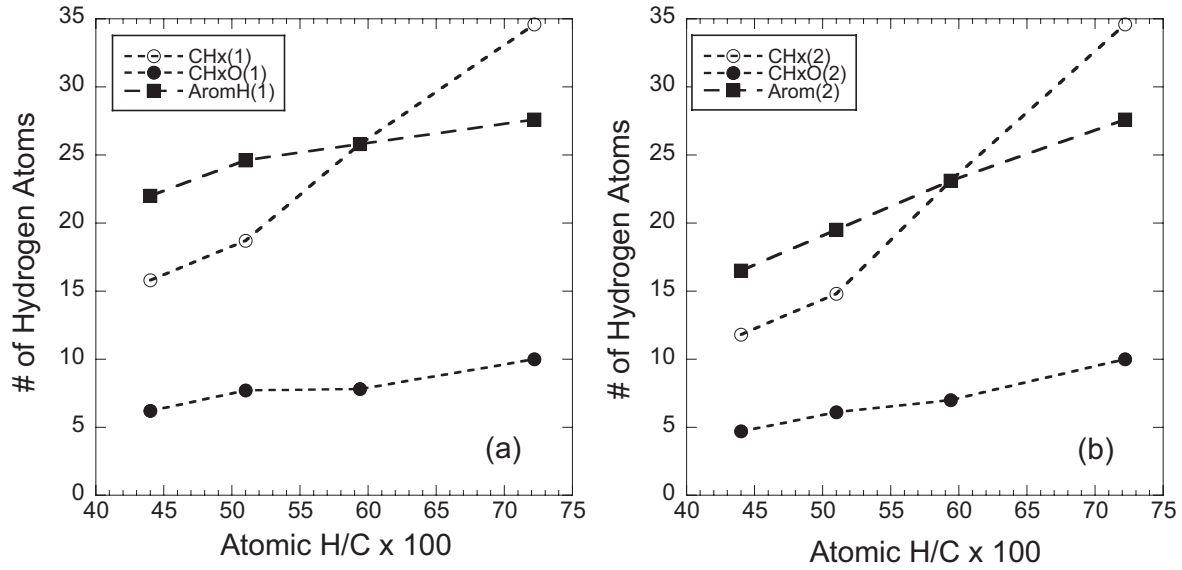

Fig. 9. Changes in the number of H atoms (normalized to 100 C atoms of starting IOM) in different functional groups as a function of bulk IOM atomic H/C ratios in (a) Model 1, and (b) Model 2. The primary consequence of choosing either a constant bulk IOM C abundance (Model 1) or a constant IOM aromatic C abundance (Model 2) is the total amount of H that is lost moving from lithology 5b to 11v, which are 39% and 54% for Model 1 and 2, respectively. In both models, all major functional groups lose H, but the greatest losses are experienced by the combined CH_x groups (methyl, methylene, and methane).

hydrothermal experiments indicate that extensive exchange does occur at least at elevated temperatures (Yabuta et al. 2007; Oba and Naraoka 2009).

Constraining the Conditions of IOM Modification

As stated above, the molecular transformation observed moving from 5b to 11v, in particular the increase in aromatic condensation, is consistent with thermally driven chemistry. Thus, the differences in IOM behavior between the Tagish Lake lithologies and among the CI-CM-CR chondrites may simply be a function of differences in the temperatures and/or timescales of alteration. If, for instance, peak temperature was the determining factor in the extent of modification in the IOM during alteration, then our results suggest that the CI and CM alteration temperatures were similar to those experienced by 11h; the CR alteration temperatures were similar to or lower than those experienced by 5b; and CI-CM-CR alteration occurred at significantly lower temperatures than for 11v and 11i. This order of alteration temperature is different from what would be predicted from the various literature estimates for alteration temperatures, which generally indicate alteration temperatures in the order CI≈CR>CM (Brearley 2006). Our results would suggest that alteration temperatures have been overestimated for the CRs and underestimated for the CMs. This could reflect the fact that some or all of the mineralogical indicators used to infer alteration temperatures were established prior to or after the peak temperatures. Also, the very similar IOM NMR spectra for both type 1 and type 2 CMs (Cody et al. 2008c) suggest that all CMs experienced similar peak temperatures, which, for the CM1s, have been estimated to be ≥120 °C (Zolensky et al. 1997). However, if kinetic factors, and not just peak temperature, are important, it is possible that longer alteration times at lower temperatures or shorter alteration times at higher temperatures can achieve similar degrees of IOM modification. To determine which is the explanation will require a detailed understanding of the kinetics of IOM structural and isotopic modification under hydrothermal conditions.

Hydrothermal (approximately 300 °C) alteration has been shown to convert IOM from the CM2s Murray and Murchison into highly aromatic residues on timescales of days (Yabuta et al. 2007; Oba and Naraoka 2009). This aromatization is accompanied by extensive H isotope exchange and the production of low molecular weight organic compounds (i.e., there is some mass loss from the IOM). Intriguingly, the Oba and Naraoka (2009) results exhibit a linear correlation between H/C and δD that roughly parallels the Tagish Lake trend (Fig. 1b). Sephton et al. (2000) also used hydrothermal alteration (320 °C for 72 h) to liberate small organic molecules from meteorite IOM. A process akin to this may have been responsible for the free PAHs found in CMs, as well as differences between CMs and CIs (Sephton et al. 2000; Sephton 2013).

In the Yabuta et al. (2007) experiments, the Murray IOM lost approximately 13% of its C, which is less than predicted by Model 2 but higher than allowed by the variations in IOM content between the Tagish Lake lithologies (Table 1, discounting 5b(2)). The Tagish Lake lithologies do contain many of the soluble species generated in the Yabuta et al. (2007) experiments (Pizzarello et al. 2001; Herd et al. 2011; Hilts et al. 2014). However, these soluble species are present at total concentrations of up to only 100s of ppm, roughly an order of magnitude lower than would be required by Model 2. Also, they are more abundant in 5b and 11h (least modified IOM) than in 11i, 11v, and the original Tagish Lake sample (most modified IOM), i.e., the opposite of what would be predicted by Model 2. It cannot be ruled out that much of the soluble material was removed from the more altered lithologies during or after alteration. Even so, temperatures that were significantly lower than 300 °C would seem to be required for the alteration of the Tagish Lake lithologies (and the other C1/2 chondrites) to explain the low mass losses implied by the relatively constant IOM C abundances in all the Tagish Lake lithologies (Table 1).

The Yabuta et al. (2007) experiments were conducted for 6 days, although the transformation could have taken less time. In a recent study of the potential origin of IOM from formaldehyde polymer, heating of the polymer at 250 °C for 4 h was required to reproduce a material that was similar in its functional group chemistry to IOM (Cody et al. 2011). To achieve the chemical and isotopic modifications of the IOM in the Tagish Lake lithologies at lower temperatures would require significantly longer alteration timescales (Alexander et al. 2010). Nevertheless, the apparently relatively facile conversion of aliphatic to aromatic material in IOM might best be explained by the extensively branched structure of the aliphatic material that minimizes the amount of C–C bond cleavage and reformation needed to achieve the transformation. For example, Cody et al. (2011) suggested that a viable route for making aromatic material at mild temperatures would be through cycloaddition reactions, requiring that substituted cyclic aliphatic groups are abundant in primitive IOM.

How was the range of conditions experienced by the four Tagish Lake lithologies achieved? It is certainly possible that the Tagish Lake meteoroid is a breccia containing fragments from quite different parts of the Tagish Lake parent body. Alternatively, such a range of thermal histories in a relatively small meteoroid—Brown et al. (2000) estimated a preatmospheric diameter of about 4–6 m—might be explained if it formed adjacent either to a fracture along which hot fluids flowed or to an igneous intrusion that induced hydrothermal activity. In this scenario, lithologies 11i and 11v would have come from closest to the fracture or intrusion. Farther away from the fracture or intrusion, the temperature would have dropped significantly, leading to the moderate thermal processing of lithology 11h, and farther away still to little or no thermal processing of lithology 5b. An impact is an alternative heat source. However, there is no evidence for shock in the Tagish Lake samples, and it remains unclear whether shock heating would have lasted long enough to produce the transformations seen in the IOM or why it produced such a range of impact heating in such a small object.

SUMMARY AND CONCLUSIONS

Four distinct Tagish Lake lithologies have been identified that experienced differing degrees of aqueous alteration. With the aim of understanding how aqueous alteration modified the IOM, IOM isolates from these lithologies have been subjected to a number of analytical techniques to determine their abundances, bulk elemental and isotopic compositions, and functional group chemistries.

The IOM in these lithologies exhibits a wide range of H/C (atom) ratios (0.427–0.766) that are linearly correlated with δD values (789–1854‰). Despite this range of compositions, the range of IOM C abundances in the four lithologies is remarkably constant. The variation in IOM compositions also correlates with petrologic estimates of the relative extents of aqueous alteration experienced by the host lithologies—the least altered has the highest H/C ratio and δD value, while the most altered has the lowest H/C ratio and δD value. IOM from a previous study of Tagish Lake extends the correlation to H/C ratios and δD values of 0.337 and 594‰, respectively. This variation in H/C ratios exhibited by the Tagish Lake IOM samples covers the range from the CRs, CIs, and CMs to the least metamorphosed OCs, CVs, and COs, and all but the most heated of the heated CMs.

The variation in H/C ratios suggests that there is a range of aromaticity in the IOM. This is clearly demonstrated by NMR and IR studies. The IOM from the least altered lithology (5b) has an aromatic C fraction, determined by NMR, of 0.55, and its ^{13}C and ^{1}H NMR spectra resemble those of IOM from CR chondrites. The NMR spectrum of the IOM from the next most primitive lithology (11h) resembles those of CM chondrite IOM. The NMR spectra of the Tagish Lake IOM with the lowest H/C are highly aromatic (aromatic C fraction ≥0.79; Cody and Alexander 2005), much like the more heated CMs and the CV3 Vigarano. However, unlike the most heated CMs and Vigarano, the Tagish Lake IOM does not show a paramagnetic

shift in its aromatic NMR peak (Cody et al. 2008b). This suggests that the Tagish Lake samples did not experience peak temperatures that were as high as those experienced by the more heated CMs, or as sustained as those experienced by the CVs during metamorphism. IR spectroscopy shows a similar variation in aromatic and aliphatic features to the NMR. When combined, the IR and NMR measurements indicate that in terms of their relative abundances $CH>>CH_2>CH_3$ in the aliphatic material in all the lithologies, and that the aliphatic material must, therefore, be composed of short, highly branched chains irrespective of the aliphatic/aromatic C ratio of the IOM.

The correlation between petrologic estimates of the degree of aqueous alteration and the chemical, isotopic, and structural properties of the IOM suggests that the aqueous alteration was responsible for the IOM variations. In this case, the precursor material most closely resembled the IOM in the least altered lithology, which has an H/C ratio and NMR spectral properties like those of CR IOM and a bulk δD value that is intermediate between CR and typical CM IOM. This interpretation is supported by experimental evidence that hydrothermal alteration does profoundly modify the chemical, isotopic, and structural properties of IOM (Yabuta et al. 2007; Oba and Naraoka 2009). The hydrothermal experiments were conducted at high temperatures (approximately 300 °C) for several days and resulted in the loss of some C from the IOM. However, there is little evidence for C loss from the IOM in Tagish Lake samples. It is possible that this is because the Tagish Lake samples experienced lower temperatures for more sustained periods of time. Nevertheless, there is some evidence for partial dehydration of the more altered lithologies, consistent with fairly elevated temperatures for some period of time.

We have considered two endmember models, both constrained by our elemental and NMR data, for how the IOM transformation might occur on a functional group chemistry level. In Model 1, aliphatic material is converted to aromatic material, conserving C but resulting in a loss of H. In Model 2, only the original aromatic C is conserved and requiring a loss of approximately 25% of the C in the most processed lithology (11i). There is no systematic loss of IOM C across the four lithologies. Hence, Model 1 seems to best explain the data, although some loss of C as the IOM was transformed cannot be ruled out.

The setting in which the alteration of the Tagish lake samples took place remains unclear. It is possible that Tagish Lake is a breccia that sampled widely dispersed regions of a globally altered parent body. However, it is also possible that the alteration was much more localized, e.g., a reaction aureole around an igneous intrusion or a fracture along which hot fluids once flowed.

Our results for Tagish Lake strongly support our previous contention that parent body processing of a CR-IOM-like precursor material was largely responsible for the diversity of IOM elemental, isotopic, and molecular compositions found in chondrites (Cody and Alexander 2005; Alexander et al. 2007, 2010). If temperature and time primarily dictated the IOM properties (as opposed to mineralogy, fluid chemistry, etc.) of aqueously altered chondrites, then CI and CM chondrites saw similarly higher peak temperatures and/or more extended periods of aqueous alteration than the CR chondrites.

Acknowledgments—We thank Scott Sandford and Corentin Le Guillou for thoughtful and thorough reviews that greatly improved this manuscript. This study was partially funded by Carnegie Institution of Canada and NASA Astrobiology (NNA09DA81A) grants (CA, RB, GC, MF, LN), by NASA grant NNX11AG67G (CA), and by Natural Sciences and Engineering Research Council of Canada grant 261740-08 (CDKH). YK gratefully acknowledges support through the JSPS Postdoctoral Fellowship program. The Advanced Light Source is a DOE facility.

Editorial Handling—Dr. Gretchen Benedix

REFERENCES

Alexander C. M. O'D. 2005. Re-examining the role of chondrules in producing the volatile element fractionations in chondrites. *Meteoritics & Planetary Science* 40: 943–965.

Alexander C. M. O'D., Russell S. S., Arden J. W., Ash R. D., Grady M. M., and Pillinger C. T. 1998. The origin of chondritic macromolecular organic matter: A carbon and nitrogen isotope study. *Meteoritics & Planetary Science* 33:603–622.

Alexander C. M. O'D., Fogel M., Yabuta H., and Cody G. D. 2007. The origin and evolution of chondrites recorded in the elemental and isotopic compositions of their macromolecular organic matter. *Geochimica et Cosmochimica Acta* 71:4380–4403.

Alexander C. M. O'D., Newsome S. N., Fogel M. L., Nittler L. R., Busemann H., and Cody G. D. 2010. Deuterium enrichments in chondritic macromolecular material—Implications for the origin and evolution of organics, water and asteroids. *Geochimica et Cosmochimica Acta* 74:4417–4437.

Alexander C. M. O'D., Bowden R., Fogel M. L., Howard K. T., Herd C. D. K., and Nittler L. R. 2012. The provenances of asteroids, and their contributions to the volatile inventories of the terrestrial planets. *Science* 337:721–723.

Alexander C. M. O'D., Bowden R., Fogel M. L., and Howard K. 2013a. Carbonate abundances and isotopic

compositions in chondrites (abstract #2788). 44th Lunar and Planetary Science Conference. CD-ROM.

Alexander C. M. O'D., Howard K., Bowden R., and Fogel M. L. 2013b. The classification of CM and CR chondrites using bulk H, C and N abundances and isotopic compositions. *Geochimica et Cosmochimica Acta* 123:244–260.

Alexander R., Kagi R. I., and Larcher A. V. 1982. Clay catalysis of aromatic hydrogen-exchange reactions. *Geochimica et Cosmochimica Acta* 46:219–222.

Blinova A. I., Herd C. D. K., and M. J. M. Duke 2014a. Testing variations within the Tagish Lake Meteorite—II: Whole-rock geochemistry of pristine samples. *Meteoritics & Planetary Science*, doi:10.1111/maps.12271.

Blinova A. I., Zega T., Herd C. D. K., and Stroud R. 2014b. Testing variations within the Tagish Lake meteorite—I: Mineralogy and petrology of pristine samples. *Meteoritics & Planetary Science*, doi:10.1111/maps.12271.

Bonal L., Quirico E., Bourot-Denise M., and Montagnac G. 2006. Determination of the petrologic type of CV3 chondrites by Raman spectroscopy of included organic matter. *Geochimica et Cosmochimica Acta* 70:1849–1863.

Bonal L., Bourot-Denise M., Quirico E., Montagnac G., and Lewin E. 2007. Organic matter and metamorphic history of CO chondrites. *Geochimica et Cosmochimica Acta* 71:1605–1623.

Brearley A. J. 1995. Aqueous alteration and brecciation in Bells, an unusual saponite-bearing, CM chondrite. *Geochimica et Cosmochimica Acta* 59:2291–2318.

Brearley A. J. 2006. The action of water. In *Meteorites and the early solar system II*, edited by Lauretta D. S. and McSween H. Y. Jr. Tucson, Arizona: The University of Arizona Press. pp. 584–624.

Brown P. G., Hildebrand A. R., Zolensky M. E., Grady M., Clayton R. N., Mayeda T. K., Tagliaferri E., Spalding R., MacRae N. D., Hoffman E. L., Mittlefehldt D. W., Wacker J. F., Bird J. A., Cambell M. D., Carpenter R., Gingerich H., Glatiotis M., Greiner E., Mazur M. J., McCausland P. J., Plotkin H., and Mazur T. R. 2000. The fall, recovery, orbit and composition of the Tagish Lake meteorite: A new type of carbonaceous chondrite. *Science* 290:320–325.

Busemann H., Young A. F., Alexander C. M. O'D., Hoppe P., Mukhopadhyay S., and Nittler L. R. 2006. Interstellar chemistry recorded in organic matter from primitive meteorites. *Science* 314:727–730.

Busemann H., Alexander C. M. O'D., and Nittler L. R. 2007. Characterization of insoluble organic matter in primitive meteorites by microRaman spectroscopy. *Meteoritics & Planetary Science* 42:1387–1416.

Busemann H., Nguyen A. N., Cody G. D., Hoppe P., Kilcoyne A. L. D., Stroud R. M., Zega T. J., and Nittler L. R. 2009. Ultra-primitive interplanetary dust particles from the comet 26P/Grigg-Skjellerup dust stream collection. *Earth and Planetary Science Letters* 288:44–57.

Cody G. D. and Alexander C. M. O'D. 2005. NMR studies of chemical structural variation of insoluble organic matter from different carbonaceous chondrite groups. *Geochimica et Cosmochimica Acta* 69:1085–1097.

Cody G. D., Alexander C. M. O'D., and Tera F. 2002. Solid state (^{1}H and ^{13}C) NMR spectroscopy of the insoluble organic residue in the Murchison meteorite: A self-consistent quantitative analysis. *Geochimica et Cosmochimica Acta* 66:1851–1865.

Cody G. D., Ade H., Alexander C. M. O'D., Araki T., Butterworth A., Fleckenstein H., Flynn G. J., Gilles M. K., Jacobsen C., Kilcoyne A. L. D., Messenger K., Sandford S. A., Tyliszczak T., Westphal A. J., Wirick S., and Yabuta H. 2008a. Quantitative organic and light element analysis of comet 81P/Wild 2 particles using C-, N-, and O- μ-XANES. *Meteoritics & Planetary Science* 43:353–366.

Cody G. D., Alexander C. M. O'D., Yabuta H., Kilcoyne A. L. D., Araki T., Ade H., Dera P., Fogel M., Militzer B., and Mysen B. O. 2008b. Organic thermometry for chondritic parent bodies. *Earth and Planetary Science Letters* 272:446–455.

Cody G. D., Fogel M. L., Yabuta H., and Alexander C. M. O'D. 2008c. The peculiar relationship between meteoritic organic molecular structure and deuterium abundance (abstract #1765). 39th Lunar and Planetary Science Conference. CD-ROM.

Cody G. D., Heying E., Alexander C. M. O'D., Nittler L. R., Kilcoyne A. L. D, Sandford S. A., and Stroud R. M. 2011. Establishing a molecular relationship between chondritic and cometary organic solids. *Proceedings of the National Academy of Sciences* 108:19,171–19,176.

Dartois E., Geballe T. R., Pino T., Cao A. T., Jones A., Deboffle D., Guerrini V., Brèchignac P., and D'Hendecourt L. 2007. IRAS 08572 + 3915: Constraining the aromatic versus aliphatic content of interstellar HACs. *Astronomy & Astrophysics* 463:635–640.

Davidson J., Busemann H., Alexander C. M. O'D., Nittler L. R., Schrader D. L., Orthous-Daunay F. R., Quirico E., Franchi I. A., and Grady M. M. 2009. Presolar SiC abundances in primitive meteorites by NanoSIMS raster ion imaging of insoluble organic matter (abstract #1853). 40th Lunar and Planetary Science Conference. CD-ROM.

De Gregorio B. T., Stroud R. M., Nittler L. R., Alexander C. M. O'D., Kilcoyne A. L. D., and Zega T. J. 2010. Isotopic anomalies in organic nanoglobules from Comet 81P/Wild 2: Comparison to Murchison nanoglobules and isotopic anomalies induced in terrestrial organics by electron irradiation. *Geochimica et Cosmochimica Acta* 74:4454–4470.

De Gregorio B. T., Stroud R. M., Cody G. D., Nittler L. R., Kilcoyne A. L. D., and Wirick S. 2011. Correlated microanalysis of cometary organic grains returned by Stardust. *Meteoritics & Planetary Science* 46:1376–1396.

Flynn G. J., Keller L. P., Feser M., Wirick S., and Jacobsen C. 2003. The origin of organic matter in the solar system: Evidence from interplanetary dust particles. *Geochimica et Cosmochimica Acta* 67:4791–4806.

Glavin D. P., Elsila J. E., Burton A. S., Callahan M. P., Dworkin J. P., Hilts R. W., and Herd C. D. K. 2012. Unusual nonterrestrial l-proteinogenic amino acid excesses in the Tagish Lake meteorite. *Meteoritics & Planetary Science* 47:1347–1364.

Gourier D., Robert F., Delpoux O., Binet L., Vezin H., Moissette A., and Derenne S. 2008. Extreme deuterium enrichment of organic radicals in the Orgueil meteorite: Revisiting the interstellar interpretation? *Geochimica et Cosmochimica Acta* 72:1914–1923.

Grady M. M., Verchovsky A. B., Franchi I. A., Wright I. P., and Pillinger C. T. 2002. Light element geochemistry of the Tagish Lake CI2 chondrite: Comparison with CI1 and CM2 meteorites. *Meteoritics & Planetary Science* 37:713–735.

Greshake A., Krot A. N., Flynn G. J., and Keil K. 2005. Fine-grained dust rims in the Tagish Lake carbonaceous chondrite: Evidence for parent body alteration. *Meteoritics & Planetary Science* 40:1413–1431.

Guo W. 2009. Carbonate clumped isotope thermometry: Application to carbonaceous chondrites and effects of kinetic isotope fractionation. PhD thesis. California Institute of Technology, Pasadena.

Guo W. and Eiler J. M. 2007. Temperatures of aqueous alteration and evidence for methane generation on the parent bodies of the CM chondrites. *Geochimica et Cosmochimica Acta* 71:5565–5575.

Herd C. D. K., Blinova A., Simkus D. N., Huang Y., Tarozo R., Alexander C. M. O'D., Gyngard F., Nittler L. R., Cody G. D., Fogel M. L., Kebukawa Y., Kilcoyne A. L. D., Hilts R. W., Slater G. F., Glavin D. P., Dworkin J. P., Callahan M. P., Elsila J. E., De Gregorio B. T., and Stroud R. M. 2011. Origin and evolution of prebiotic organic matter as inferred from the Tagish Lake meteorite. *Science* 332:1304–1307.

Herd C. D. K., Sharp Z. D., Alexander C. M. O'D., and Blinova A. 2012. Oxygen isotopic composition of Tagish Lake lithologies: Insights into parent body alteration (abstract #1688). 43rd Lunar and Planetary Science Conference. CD-ROM.

Hilts R. W., Herd C. D. K., Simkus D. N., and Slater G. F. 2014. Soluble organic compounds in the Tagish Lake meteorite. *Meteoritics & Planetary Science*, doi:10.1111/maps.12272.

Huss G. R., Meshik A. P., Smith J. B., and Hohenberg C. M. 2003. Presolar diamond, silicon carbide, and graphite in carbonaceous chondrites: Implications for thermal processing in the solar nebula. *Geochimica et Cosmochimica Acta* 67:4823–4848.

Jacobsen C., Flynn G. J., Wirick S., and Zimba C. 2000. Soft X-ray spectroscopy from image sequences with sub-100 nm spatial resolution. *Journal of Microscopy* 197:173–184.

Jiang Y. J., Solum M. S., Pugmire R. J., Grant D. M., Schobert H. H., and Pappano P. J. 2002. A new method for measuring the graphite content of anthracite coals and soots. *Energy & Fuels* 16:1296–1300.

Kebukawa Y., Nakashima S., Ishikawa M., Aizawa K., Inoue T., Nakamura-Messenger K., and Zolensky M. E. 2010. Spatial distribution of organic matter in the Bells CM2 chondrite using near-field infrared microspectroscopy. *Meteoritics & Planetary Science* 45:394–405.

Kebukawa Y., Alexander C. M. O'D., and Cody G. D. 2011. Compositional diversity in insoluble organic matter in type 1, 2 and 3 chondrites as detected by infrared spectroscopy. *Geochimica et Cosmochimica Acta* 75:3530–3541.

Keller L. P., Messenger S., Flynn G. J., Clemett S., Wirick S., and Jacobsen C. 2004. The nature of molecular cloud material in interplanetary dust. *Geochimica et Cosmochimica Acta* 68:2577–2589.

Kerridge J. F. 1983. Isotopic composition of carbonaceous-chondrite kerogen: Evidence for an interstellar origin of organic matter in meteorites. *Earth and Planetary Science Letters* 64:186–200.

Kilcoyne A. L. D., Tyliszczak T., Steele W. F., Fakra S., Hitchcock P., Franck K., Anderson E., Harteneck B., Rightor E. G., Mitchell G. E., Hitchcock A. P., Yang L., Warwick T., and Ade H. 2003. Interferometer controlled scanning transmission microscopes at the advanced light source. *Journal of Synchrotron Radiation* 10:125–136.

Kissel J., and Krueger F. R. 1987. The organic component in dust from comet Halley as measured by the PUMA mass spectrometer on board Vega 1. *Nature* 326:755–760.

Le Guillou C., Rouzaud J.-N., Bonal L., Quirico E., Derenne S., and Remusat L. 2012. High resolution TEM of chondritic carbonaceous matter: Metamorphic evolution and heterogeneity. *Meteoritics & Planetary Science* 47:345–362.

Matrajt G., Borg J., Raynal P. I., Djouadi Z., d'Hendecourt L., Flynn G., and Deboffle D. 2004. FTIR and Raman analyses of the Tagish Lake meteorite: Relationship with the aliphatic hydrocarbons observed in the diffuse interstellar medium. *Astronomy & Astrophysics* 416:983–990.

Matrajt G., Ito M., Wirick S., Messenger S., Brownlee D. E., Joswiak D., Flynn G., Sandford S., Snead C., and Westphal A. 2008. Carbon investigation of two Stardust particles: A TEM, NanoSIMS, and XANES study. *Meteoritics & Planetary Science* 43:315–334.

Matrajt G., Messenger S., Brownlee D., and Joswiak D. 2012. Diverse forms of primordial organic matter identified in interplanetary dust particles. *Meteoritics & Planetary Science* 47:525–549.

Messenger S. 2000. Identification of molecular-cloud material in interplanetary dust particles. *Nature* 404:968–971.

Mittlefehldt D. W. 2002. Geochemistry of the ungrouped carbonaceous chondrite Tagish Lake, the anomalous CM chondrite Bells, and comparison with CI and CM chondrites. *Meteoritics & Planetary Science* 37:703–712.

Nakanishi K. and Solomon P. H. 1977. *Infrared absorption spectroscopy*. Boca Raton, Florida: Emerson-Adams Press. 287 p.

Nuth J. A. III, Johnson N. M., and Manning S. 2008. A self-perpetuating catalyst for the production of complex organic molecules in protostellar nebulae. *The Astrophysical Journal Letters* 673:L225–L228.

Oba Y. and Naraoka H. 2003. A different behavior of hydrogen isotope exchange in aqueous solutions between two PAH isomers (fluoranthene and pyrene). *Research in Organic Geochemistry* 18:29–35.

Oba Y. and Naraoka H. 2009. Elemental and isotopic behavior of macromolecular organic matter from CM chondrites during hydrous pyrolysis. *Meteoritics & Planetary Science* 44:943–954.

Orthous-Daunay F. R., Quirico E., Beck P., Brissaud O., Dartois E., Pino T., and Schmitt B. 2013. Mid-infrared study of the molecular structure variability of insoluble organic matter from primitive chondrites. *Icarus* 223:534–543.

Pearson V. K., Sephton M. A., Franchi I. A., Gibson J. M., and Gilmour I. 2006. Carbon and nitrogen in carbonaceous chondrites: Elemental abundances and stable isotopic compositions. *Meteoritics & Planetary Science* 41:1899–1918.

Piani L., Robert F., Beyssac O., Binet L., Bourot-Denise M., Derenne S., Le Guillou C., Marrocchi Y., Mostefaoui S., Rouzaud J.-N., and Thomen A. 2012. Structure, composition, and location of organic matter in the enstatite chondrite Sahara 97096 (EH3). *Meteoritics & Planetary Science* 47:8–29.

Pizzarello S., Huang Y., Becker L., Poreda R. J., Nieman R. A., Cooper G., and Williams M. 2001. The organic content of the Tagish Lake meteorite. *Science* 293:2236–2239.

Pretsch E., Bühlmann P., and Affolter C. 2000. *Structure determination of organic compounds*. New York: Springer. 441 p.

Quirico E., Raynal P. I., and Bourot-Denise M. 2003. Metamorphic grade of organic matter in six unequilibrated ordinary chondrites. *Meteoritics & Planetary Science* 38:795–811.

Quirico E., Montagnac G., Rouzaud J. N., Bonal L., Bourot-Denise M., Duber S., and Reynard B. 2009. Precursor and metamorphic condition effects on Raman spectra of poorly ordered carbonaceous matter in chondrites and coals. *Earth and Planetary Science Letters* 287:185–193.

Remusat L., Palhol F., Robert F., Derenne S., and France-Lanord C. 2006. Enrichment of deuterium in insoluble organic matter from primitive meteorites: A solar system origin? *Earth and Planetary Science Letters* 243:15–25.

Ristein J., Stief R. T., and Ley L. 1998. A comparative analysis of a-C: H by infrared spectroscopy and mass selected thermal effusion. *Journal of Applied Physics* 84:3836–3847.

Robert F. and Epstein S. 1982. The concentration and isotopic composition of hydrogen, carbon and nitrogen in carbonaceous meteorites. *Geochimica et Cosmochimica Acta* 46:81–95.

Sandford S. A., Aléon J., Alexander C. M. O'D., Araki T., Bajt S., Baratta G. A., Borg J., Bradley J. P., Brownlee D. E., Brucato J. R., Burchell M. J., Busemann H., Butterworth A., Clemett S. J., Cody G., Colangeli L., Cooper G., d'Hendecourt L., Djouadi Z., Dworkin J. P., Ferrini G., Fleckenstein H., Flynn G. J., Franchi I. A., Fries M., Gilles M. K., Glavin D. P., Gounelle M., Grossemy F., Jacobsen C., Keller L. P., Kilcoyne A. L. D., Leitner J., Matrajt G., Meibom A., Mennella V., Mostefaoui S., Nittler L. R., Palumbo M. E., Papanastassiou D. A., Robert F., Rotundi A., Snead C. J., Spencer M. K., Stadermann F. J., Steele A., Stephan T., Tsou P., Tyliszczak T., Westphal A. J., Wirick S., Wopenka B., Yabuta H., Zare R. N., and Zolensky M. E. 2006. Organics captured from comet 81P/Wild 2 by the Stardust spacecraft. *Science* 314:1720–1724.

Sephton M. A. 2013. Aromatic units from the macromolecular material in meteorites: Molecular probes of cosmic environments. *Geochimica et Cosmochimica Acta* 107:231–241.

Sephton M. A., Pillinger C. T., and Gilmour I. 2000. Aromatic moieties in meteoritic macromolecular materials: analyses by hydrous pyrolysis and δ^{13} C of individual compounds. *Geochimica et Cosmochimica Acta* 64:321–328.

Socrates G. 2001. *Infrared and Raman characteristic group frequencies*. Chichester: John Wiley & Sons. p. 366.

Van Krevelen D. W. 1993. *Coal*. New York: Elsevier. 979 p.

Yabuta H., Williams L. B., Cody G. D., Alexander C. M. O'D., and Pizzarello S. 2007. The insoluble carbonaceous material of CM chondrites: A possible source of discrete organic compounds under hydrothermal conditions. *Meteoritics & Planetary Science* 42:37–48.

Yang J. and Epstein S. 1983. Interstellar organic matter in meteorites. *Geochimica et Cosmochimica Acta* 47:2199–2216.

Yang J. and Epstein S. 1984. Relic interstellar grains in Murchison meteorite. *Nature* 311:544–547.

Zolensky M. E., Bourcier W. L., and Gooding J. L. 1989. Aqueous alteration on the hydrous asteroids—Results of EQ3/6 computer simulations. *Icarus* 78:411–425.

Zolensky M. E., Mittlefehldt D. W., Lipschutz M. E., Wang M.-S., Clayton R. N., Mayeda T. K., Grady M. M., Pillinger C. T., and Barber D. J. 1997. CM chondrites exhibit the complete petrologic range from type 2 to 1. *Geochimica et Cosmochimica Acta* 61:5099–5115.

Zolensky M. E., Nakamura K., Gounelle M., Mikouchi T., Kasama T., Tachikawa O., and Tonui E. 2002. Mineralogy of Tagish Lake: An ungrouped type 2 carbonaceous chondrite. *Meteoritics & Planetary Science* 37:737–761.